Characterization and Optimization of Temperature-Sensitive Microbeads for Simultaneous Thermometry and Velocimetry for Fluid Dynamic Applications

Trey Cottingham

A thesis submitted in partial fulfillment of the
requirements for the degree of

Master of Science in Aeronautics & Astronautics

University of Washington

2015

Reading Committee:

Dana Dabiri, Chair

Gamal Khalil

Program Authorized to Offer Degree:
UW Aeronautics and Astronautics

University of Washington

Abstract

Characterization and Optimization of Temperature-Sensitive Microbeads for Simultaneous Thermometry and Velocimetry for Fluid Dynamic Applications

Trey Cottingham

Chair of the Supervisory Committee:
Associate Professor Dana Dabiri
UW Aeronautics and Astronautics

Luminescent paint is an established method for measuring both pressure and temperature distributions on surfaces. These Temperature-Sensitive Paints (TSP) and Pressure-Sensitive Paints (PSP) are commercially available and used regularly in the study of fluids. New microbeads using temperature-sensitive dyes were developed for applications in wind and water tunnel measurement. A novel method was developed to measure their response times to temperature changes. Their sensitivity to temperature change was also measured. A new optical system and software suite were developed. Methods for reducing spatial variations due to excitation energy were also developed.

TABLE OF CONTENTS

LIST OF FIGURES

LIST OF TABLES

GLOSSARY

PSP: Pressure-sensitive paint, a method for spatially measuring pressure on a surface

TSP: Temperature-sensitive paint, a method for spatially measuring temperature on a surface

PIV: Particle image velocimetry, a method for measuring velocity distributions in a flow.

UV: Ultraviolet light, light with wavelengths just shorter than visible range used to excite luminescence

ACKNOWLEDGMENTS

The author wishes to express sincere appreciation to University of Washington, where he has had the opportunity to work with truly professional and motivated scientists and engineers. He would also like to thank Professor Dana Dabiri and Professor Gamal Khalil for their direction and advice in this undertaking. He would also thank Dr. Wei-Hsin Tien for his mentorship and and help with this project. He would also like to thank Roy Olund of the UW Chemistry Electronics Shop for his assistance with the experimental aspects of this research. Finally, thanks are given to Lillian Pryor, Josh Hunt, and Mikko Johnson for their help in conducting the research.

DEDICATION

to my lovely wife, Sara, for letting me pursue my dreams.

Chapter 1
INTRODUCTION

Temperature, Pressure, and Velocity represent three of the fundamental fluid parameters needed to understand fluid motion and interaction. With the addition of density and various fluid constants, a complete understanding of a flow can be established. Therefore, the measurement of these three parameters is paramount in fluid measurement. Current fluid measurement techniques are still sub-optimal for measuring these parameters. Measurement techniques can be evaluated on accuracy, resolution, and intrusiveness to the flow.

1.1 Thermometry

1.1.1 Traditional Temperature Measurement

Traditionally, temperature was measured with liquid filled glass thermometers. These thermometers worked based off of the expansion of the contained liquid with changes in temperature. These temperature sensors are widely unused in modern experimentation because of the space required to transport mercury filled tubes out of the test area to a location where the thermometers can be read.[1] Along with environmental concerns,[2] these complications mean that thermometers have largely been replaced.

Thermocouples take advantage of the voltage produced between two semiconductors when a temperature gradient exists from one point of contact to another. This is known at the Seebeck effect.[3–5] The voltage is proportional to the temperature gradient and thus can be used to measure temperature. An example of several ther-

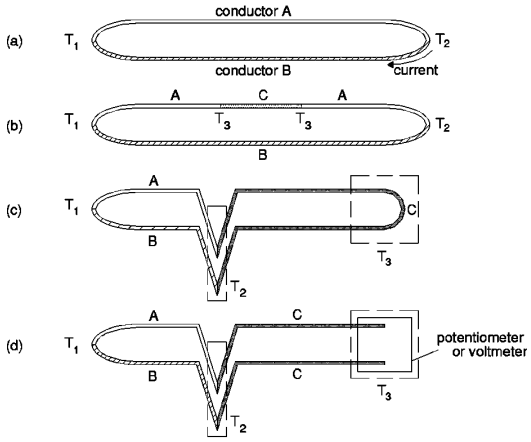

Figure 1.1: Thermocouple Circuit Development[3]

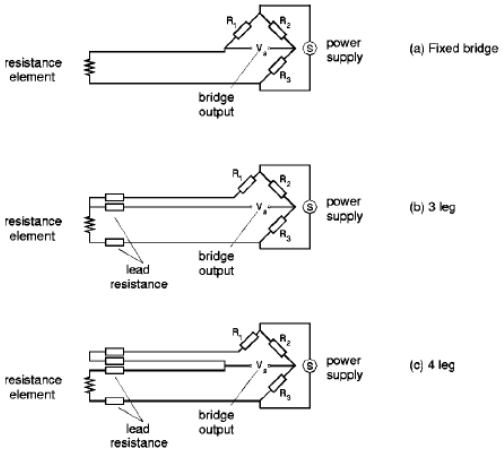

Figure 1.2: Resistance Temperature Devices[1]

mal couple circuits can be seen in Figure 1.1. This voltage can be transported easily through electric wire and digitized.[1,2,4] This makes the thermocouple a much more effective temperature sensor from an experimental point of view.

Another method of measurement requires the use of a resistive temperature device, or thermistor. These devices work based off the dependence of electrical resistance to temperature. By measuring the change in resistance of the thermistor, the temperature can be determined.[1,5] Several thermistor wiring options are shown in Figure 1.2. One limitation of thermocouples and thermistors measurement is the limited spatial resolution available. Spatial resolution is limited to the number of thermocouples or thermistors embedded in the measurement surface. Thermocouples or thermistors are largely used in modern testing where resolution is not required. Another problem with this type of measurement is the necessity to transfer the data from the measurement location through some form of electrical wire. This limits measurement to locations where direct contact is possible from an exterior probe.

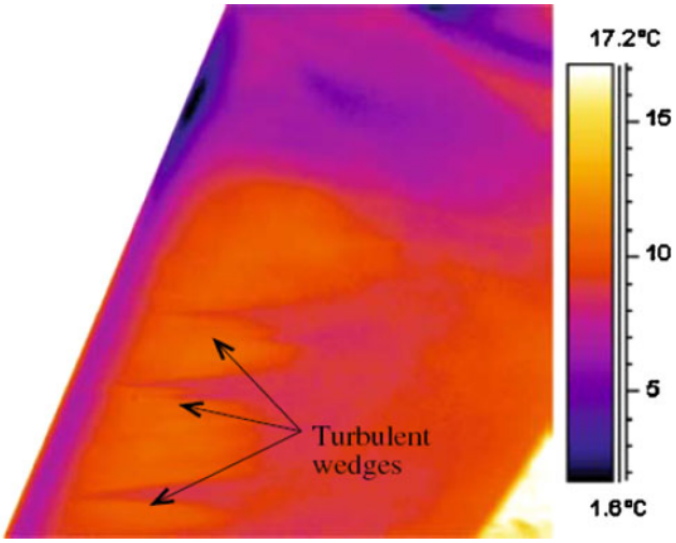

Figure 1.3: An example of IT thermometry with supersonic flow over an airfoil[7]

1.1.2 Optical Temperature Measurement

Optical measurement of temperature offers the advantage of non-contact measurement with high spatial resolution. Various optical thermometry systems exist. The first optical measurement systems were infrared thermometers.[2,6] These work off of measurement of black body radiation emitted by surfaces due to absolute temperature. IR thermometers are highly accurate and have good spatial resolution. An example of one use of IR thermometry can be seen in Figure 1.3. One major weakness to the IR thermography is that IR light does not pass through glass windows easily. This means that special windows must be manufactured to allow IR Thermography. This can be difficult as the window materials can be much harder to work with than glass.

Another optical thermometry method uses liquid crystals. By recording the alignment of the liquid crystals it is possible to relate temperature to the reflected light wavelength off of the liquid crystals. The alignment of liquid crystals determines the

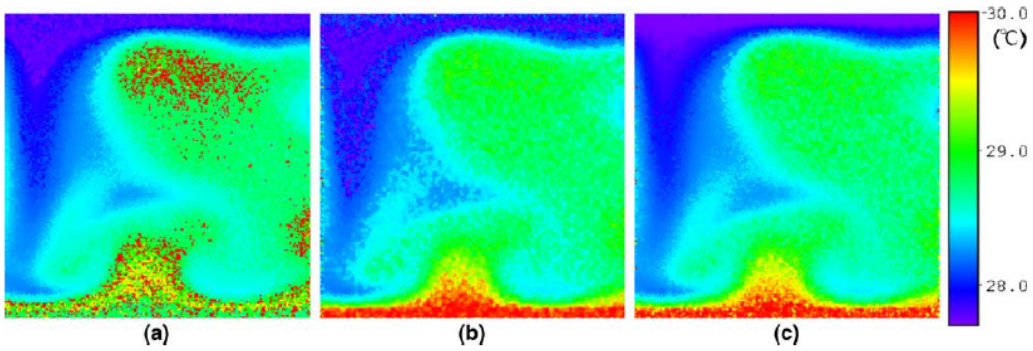

Figure 1.4: An example of liquid crystal thermometry with different calibration techniques[11]

wavelength of light reflected by the liquid crystals[8,9] and the alignment can be related to the temperature.[10] The reflected wavelength can be mapped to temperature and therefore can act as a temperature sensor with high spatial resolution. An example of this can be seen in Figure 1.4.

1.1.3 Temperature-sensitive Paint

Another method of spatially mapping temperature or heat transfer is temperature-sensitive paint (TSP). This measurement method uses luminescent dye embedded in a polymer to detect changes in temperature on the surface. The paint is excited by a UV light source which causes luminescent molecules in the paint to emit light through photo-luminescence. An example setup of this method can be seen in Figure 1.5. This luminescence can be temperature-sensitive under the right conditions.

The temperature dependence of TSPs are based off of a process called luminescent quenching. Thermal quenching occurs when increased temperature allows for alternative (non-radiative) routes of energy emission for excited luminophores. This temperature dependence causes the luminescence of the paint to change with changes in temperature. By measuring the change in luminescence, it is possible to determine a relationship with changes in temperature and therefore record temperature

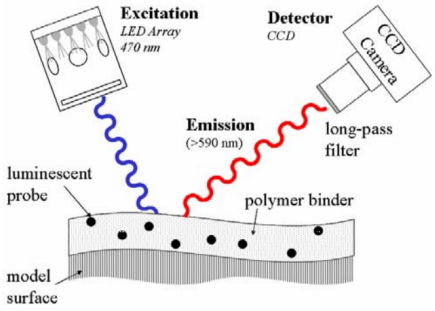

Figure 1.5: Typical setup for TSP used in experimentation[12]

distributions with high spatial resolution.

The luminescence changes can occur in either intensity or decay lifetime.[13] Different TSP methods have been developed to track these two luminescent changes. In the intensity method, the brightness of the emission is tracked with very sensitive cameras to determine temperature. In the lifetime method, the duration of the emission is tracked with very short laser pulses and fast cameras.[14] Both methods have advantages and disadvantages. The lifetime method has limited exposure time for both the camera and the laser pulse. This means that the lifetime method results in much dimmer images and requires bright dyes for use. The intensity method uses longer exposure times and thus allows for dimmer (potentially more sensitive) dyes to be used. The intensity method has issues with non-homogeneous luminophore distributions, surface irregularities, and non-uniform illumination distribution effecting the emission intensity. The lifetime method accounts for these irregularities as they do not effect the lifetime of the emission. To compensate for the spatial irregularities a reference is needed for the intensity method. This is most often a reference image taken in a known test condition. Another method of compensation utilizes a separate luminophore incorporated into the paint that is temperature insensitive to reference against. The intensity method is the focus of the research presented here.

This method is well established and commercially available.[12] Studies have been

Figure 1.6: Response of a temperature-sensitive paint to a temperature gradient on a flat surface. The plate was heated and then one end was dipped in ice water. The dark end is hot and the bright (orange) end is cold[2]

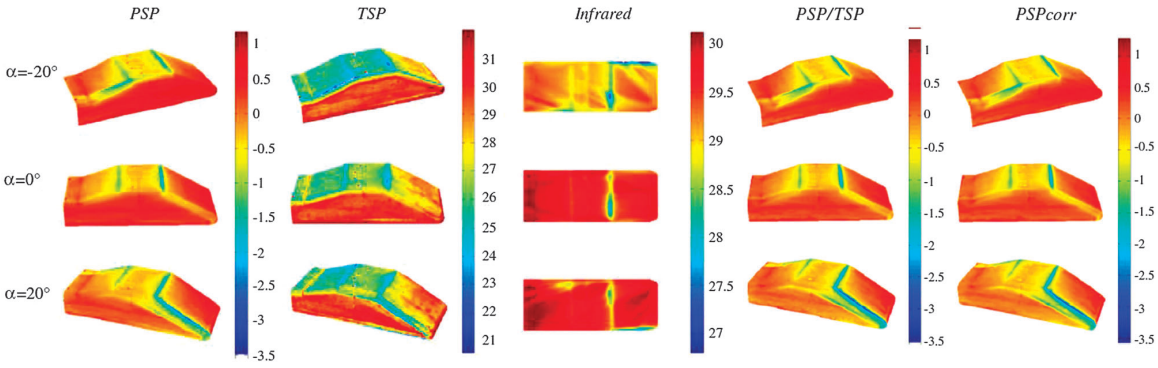

Figure 1.7: TSP is often used to account for temperature sensitivity in pressure-sensitive paint. In this case, both TSP and IR imaging were utilized to correct a PSP image.[2]

conducted in making paints thinly to allow for the conservation of surface roughness effect.[15] The applications of TSP have been studied in cryogenic testing,[16] microchannel flow,[17] unsteady flows,[18] high temperature flows,[15] and for bio-medical applications.[19] Studies have investigated minimizing the time response,[20] maximizing the temperature sensitivity,[21] and increasing the overall intensity of TSPs.[21] A review discussing the overall principles of surface temperature measurement with phosphors embedded in a polymer matrix is presented by Brübach *et. al.*[22] An example of TSP imaging can be seen in Figure 1.6. TSP is often used to correct for temperature sensitivity in PSPs. Using the temperature-sensitive paint to ind the temperature over a model, this can be used to detrend a pressure image with respect to temperature. An example of this can be seen in Figure 1.7.

1.2 Particle Image Velocimetry

Particle image velocimetry (PIV) uses a laser sheet to illuminate particles injected into a flow field. These particles have sufficiently low Stokes number to follow the streamlines of the flow. By taking two images separated by a short period of time, the motion of the particles can be determined and used to determine a velocity field in the flow. In PIV, this is done by cross-correlating interrogation windows of the images. This cross-correlation results in an average displacement for the interrogation window which when combined with the known time lapse between the image pairs determines the velocity field. PIV is a well established technique in the analysis of fluid flows. It is used most prominently in the analysis of two-dimensional turbulent flows. A typical PIV setup is shown in Figure 1.8.

1.3 Motivation - Simultaneous Temperature and Velocity Measurement

The logical next step in these developments is to combine the methods to measure temperature and velocity simultaneously. This would allow for the measurement of turbulent thermofluidic flows where both velocity and temperature are varying in

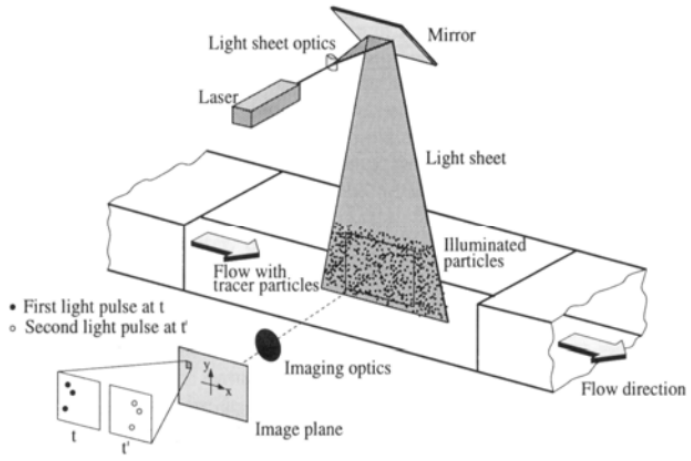

Figure 1.8: Typical layout of PIV setup for use in experimentation[23]

the flow field with time.[24] This could be done by dying the seeding particles or microbeads used in PIV with the temperature-sensitive dye combinations used for TSP. With sufficient illumination and emission, these particles could provide both temperature and velocity data globally in a flow field.

Full field thermometry and velocimetry has been attempted before with various other methods. Thermochromic liquid crystals (TLC) were shown to be effective in such measurement. TLC's work by shining a white light source on encapsulated liquid crystals. The reflected color spectrum is measured and used to determine the temperature of the flow field. An example setup for this type of experiment can be seen in Figure 1.9. The encapsulated TLC's can also serve as tracer particles for PIV.[10,25] The results of this can be seen in Figure 1.10. In this example the liquid crystals provide temperature data and the droplets are traced to measure velocity. This approach is better suited for fluid flows with very small temperature changes, however, because the temperature sensitivity of thermochromic liquid crystals is based on the color scattering temperature range and this range is often very small.

A method has been implemented where the luminescent lifetime of temperature-

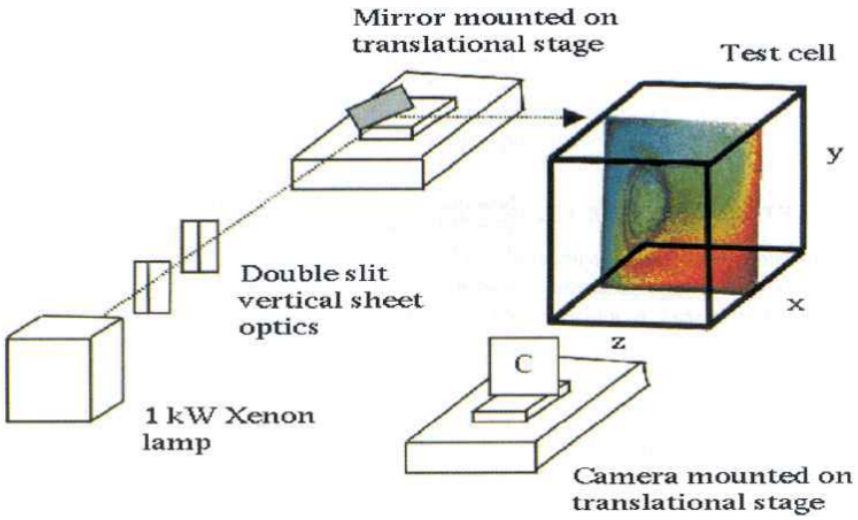

Figure 1.9: Liquid Crystal thermography and PIV setup example[25]

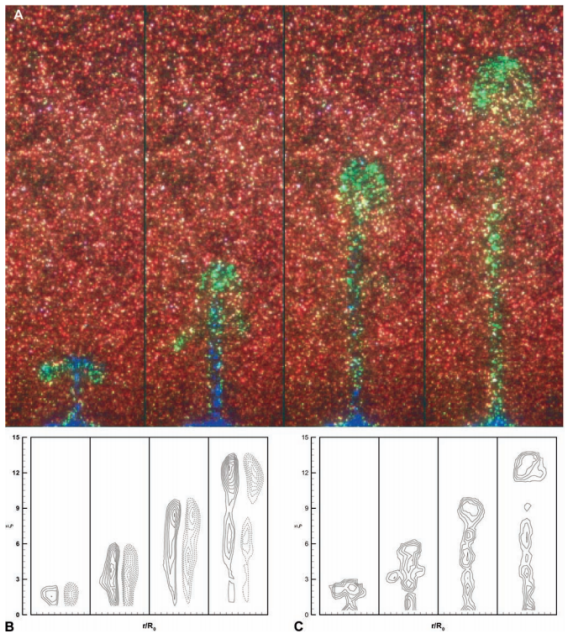

Figure 1.10: Liquid Crystal thermography and PIV Result Example.[26] **a** The color of the reflectance correlates to temperature. **b** Contours of constant vorticity are found from the velocity data. **c** temperature contours are drawn from the color of the reflectance.

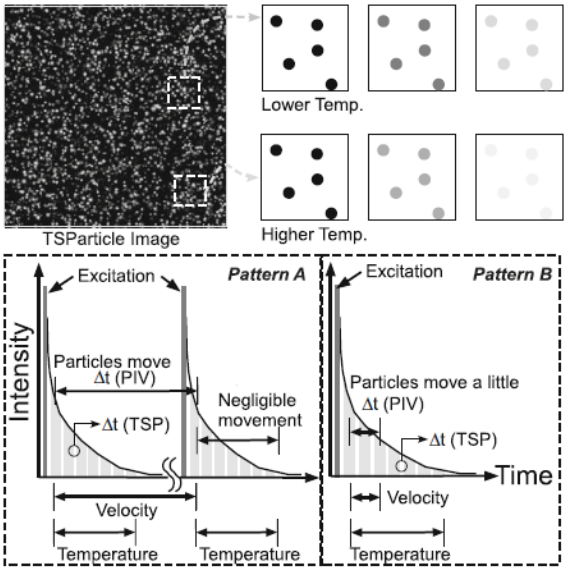

Figure 1.11: Concept of lifetime based TSP method.[29] Higher temperatures result in a shorter luminescent lifetime. With multiple exposures, this lifetime can be measured and related to temperature throughout the flow field. Particle images also allow for PIV.

sensitive luminescent particles were utilized for simultaneous PIV and thermometry.[27–29] The basic concept of this idea can be seen in Figure 1.11. The luminescent lifetime of the dye emission is temperature dependent. When hot, the lifetime of the dye is short and when cold the lifetime is longer. For this method, a series of images are taken after excitation to record the drop in emission intensity. It is assumed that during this time the motion of the particles is negligible. A Europium complex (EuTTA) was used to dope PIV particles which were sent through a heated oil flow. However, the constraints on the time limit of exposure limit the use of this technique may limit it's use in some turbulent flows. The limit on the maximum exposure time prevents many dyes from being used as only the brightest dyes emit enough light during short exposures to provide good images.

Our group at the University of Washington has conducted some research into the use of the intensity method of measurement for use in simultaneous thermometry and

PIV. The concept was proven and work was conducted to measure the temperature sensitivity and to fit suitable dyes into the emission spectrum.[24,30,31] Tests were conducted to carefully select the particle material, particle size, and luminescent dyes. Particles were tested and evaluated but full optimization had not yet been conducted. To fully determine a suitable dye, the temperature response time was needed.

Chapter 2

THEORY

Much of the theory behind temperature-sensitive microbeads is developed from existing practices and theory of its parent technologies. The luminescent theory is largely derived from the luminescent theory in temperature-sensitive and pressure-sensitive paints. PIV theory is already well established in experimentation. The particles must exhibit properties that will make them both successful temperature sensors and successful PIV tracers. For luminescent temperature sensitivity, these properties are temperature sensitivity, temperature time response, and suitable spectrum for both temperature and reference dyes. For PIV, the particles must have suitable size and density.

2.1 Luminescence

It is first necessary to address the source of dye luminescence. The various relaxation transitions are shown in the Jabloński diagram in Figure 2.1. The molecules in the dye are excited by a UV light source which raises them from their ground state to an excited singlet state (S_1, S_2, etc.) Almost instantaneously, the excited molecule will relax to the S_1 state. From the S_1 state there are multiple relaxation pathways for the energy to be released. The particle can relax through internal conversion of the energy producing no luminescence. The molecule can also fluoresce and proceed directly back down to S_0. This produces a light emission at a longer wavelength than absorbed. The third pathway of relaxation is an intersystem crossing to a triplet state (T_1). This pathway is forbidden according to quantum mechanics because of the requirement of spin change. The transition is only attainable due to spin-orbit

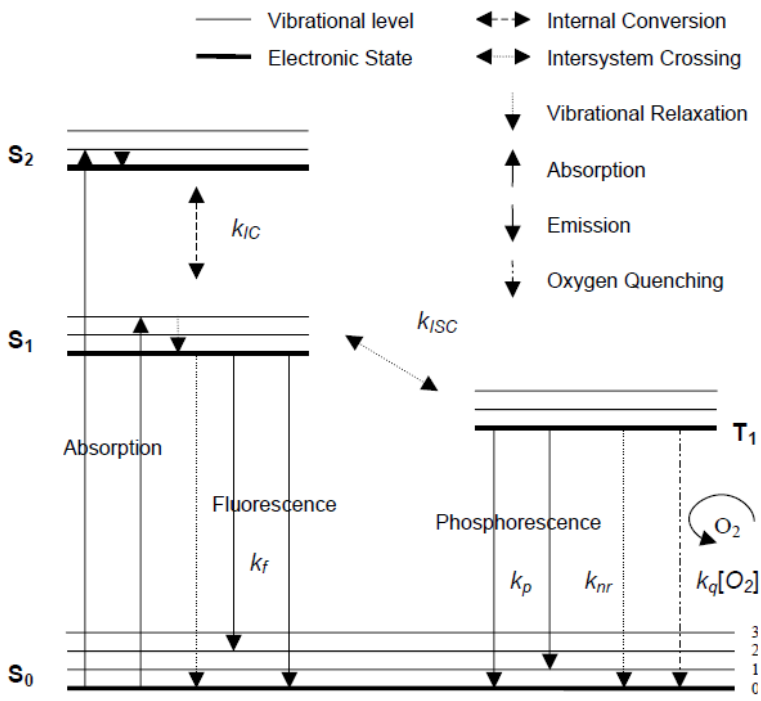

Figure 2.1: Jabloński diagram which shows all transitions of energy state[33]

coupling.[32] From the triplet state the luminophore can emit through phosphorescence or relax through non-radiative dacay. Luminescent dyes can be either phosphorescent or fluorescent. Fluorescent dyes are faster but have a broader emission spectra making them harder to combine with other dyes. Phosphorescent dyes are slower but have narrow emission spectra allowing the utilization of many of them on a single particle.

The quantum yield of a luminophore is a ratio of the emitted light to the absorbed light. The quantum yield can be quenched, or reduced, through several processes. These quenching processes allow more non-radiative relaxation of either the S_1 or T_1 states which reduces the photon emission, causing the luminescence to dim. Temperature quenching occurs when higher temperature levels allow for more relaxation through non-radiative routes. The higher temperature produces more collisions between molecules which results in more possibilities for relaxation through

non-radiative conversion.[34] This process allows for the use of some luminophores as temperature sensors. It can also cause problems for dyes designed to measure other properties such as pressure-sensitive luminophores (accounting for this form of quenching in PSP is one of the major driving factors for TSP).

Another form of quenching occurs when a luminophore comes into contact with a molecule that can easily accept the energy. Oxygen is an excellent quencher due to the triplet nature of it's molecular structure. When oxygen comes into contact with some luminophores, the oxygen takes some energy from the luminophore and reduces the rate of luminescence. This is known as oxygen quenching and is the primary mechanism for pressure-sensitive paints. Oxygen quenching is avoided when choosing temperature-sensitive luminophores to reduce variation. Temperature and oxygen quenching is modeled with the Stern-Volmer equation and when ratioed to a wind-off or reference state reads:

$$\frac{I_0}{I} = \frac{\tau_0}{\tau} = \frac{\Phi_0}{\Phi} = 1 + k_q \tau_0 [Q], \tag{2.1}$$

where I is the intensity, τ is the luminescent lifetime, and Φ is the quantum yield. The subscript 0 denotes the reference state, or zero quenched state. k_q is the rate constant of the quenching process and $[Q]$ is the rate of change of the quencher. This shows that the change in both the luminescent intensity and the luminescent lifetime are proportional to the change in quantum yield. This change is a direct result of the rate of change of the quencher concentration (which can be modeled for either temperature or oxygen quenching).

For a good temperature-sensitive particle it is necessary to find a luminescent dye that is temperature-sensitive but not oxygen sensitive. Oxygen sensitivity can be nullified if the luminophore is contained in an oxygen-impermeable binder or used in a situation where oxygen concentration does not change drastically (ie. a water tunnel). A good choice as a temeprature sensitive luminophore is europium (III) thenoyltrifluoroacetonate or EuTTA shown in Figure 2.2.

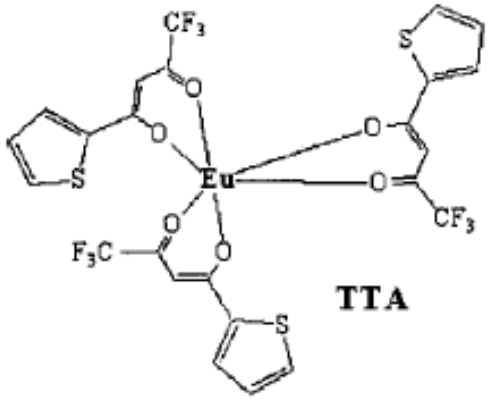

Figure 2.2: Europium III thenoyltrifluoroacetonate (EuTTA) molecule[13]

2.2 Temperature Sensitivity

Temperature sensitivity is one of the primary measures of merit for evaluating dyed microbeads. This property is the most important in determining the temperature resolution of the particles. The microbeads have to show significant change in luminescence with a change in temperature. The Stern-Volmer equation relates the temperature quenching to luminescent intensity as seen in Eq. 2.1. This relationship provides the empirical basis for the sensitivity to temperature changes. The greater the rate constant of quenching, the more sensitive the particle is to temperature changes. The higher the sensitivity, the better the particle is at sensing small changes in temperature. It is also important for the temperature sensitivity to be regular and predictable. A linear temperature sensitivity is most useful and is desirable, however, a non-linear sensitivity may be used if accounted for.

2.3 Temperature Time Response

While the temperature resolution of the particles is important, the particles must also respond quickly to changes in temperature. The temperature time response,

τ_T, of a particle is defined as the time it takes to measure 63.2% of a change in temperature.[24] While not the case anymore, this was traditionally determined by plunging a temperature sensor from ice water (0 °C) to boiling water (100 °C) and recording the time for the sensor to reach 63.2 °C. In order to fully resolve the temperatures in a flow, the temperature time response must be faster than the fastest possible change in temperature in the flow. The fastest temperature changes are going to occur in the smallest eddies of a turbulent flow. These eddies act on the order of the Kolmogorov time scale:

$$\tau_\eta = \sqrt{\frac{\nu}{\epsilon}}, \tag{2.2}$$

where ν is the kinematic viscosity and ϵ is the mean rate of viscous dissipation of the mean kinetic energy per unit mass.[24] For turbulent water tunnel experiments, $\tau_\eta \approx 100\mu$s. This sets the useful limit for particle temperature time response.

A theoretical approach to determining the temperature time response of a particle starts by modeling the heat transfer in the particle. If it is assumed that the temperature in the particle is uniform and that the radiative effects are minimal, the temperature response in the particle can be expressed in terms of the difference in temperature between the particle and the fluid:

$$mc_p\frac{dT_p}{dt} = Nu\pi k_f D(T - T_p) \tag{2.3}$$

In this equation, Nu is the Nusselt number, c_p is the specific heat of the particle material, D is the particle diameter, and k_f is the thermal conductivity of the fluid phase.[35] It is important to note that the Nusselt number in this case is an average property for the particle where:

$$Nu = \frac{hL}{k_f}$$

where h is the convective heat transfer coefficient of the fluid and L is the characteristic length of the particle. The Nusselt number is typically empirically modified for convective correlation heat transfer from spheres based on the Ranz Marshall

correlation:[36]

$$Nu = 2 + 0.6\sqrt{Re_p}\sqrt[3]{Pr}$$

Another important note is that the assumption of uniform particle temperature is based off of the calculation of the Biot number. The Biot number is the ratio of the particle internal heat transfer resistance to the particle surface heat transfer resistance.[37]

$$Bi = \frac{hL}{k_p}$$

The key distinction between the Nusselt number and the Biot number is the use of the thermal conductivity of the fluid (k_f) in the Nusselt number and the thermal conductivity of the particle (k_p) in the Biot number. If the Biot number is sufficiently less than 1 ($Bi \ll 1$) then it can reasonably be assumed that the temperature within the particle or droplet is uniform.

Dividing Equation 2.3 through by the specific heat and mass results in:[35]

$$\frac{dT_p}{dt} = \frac{Nu}{2}\frac{12k_f}{\rho_p c_p D^2}(T - T_p) \tag{2.4}$$

In low Reynolds number flows, the Nusselt number goes to 2.[35] This leaves the temperature response time:

$$\tau_T = \frac{\rho_p c_p D^2}{12k_f} \tag{2.5}$$

and the temperature response equation:

$$\frac{dT_p}{dt} = \frac{1}{\tau_T}(T - T_p) \tag{2.6}$$

This theoretical temperature response time is the time it takes the heat to dissipate in the particle and does not reflect the response of the dye itself. While this provides a good theoretical basis for determining which particles may respond faster, there are several considerations that must be noted when addressing the luminescent response time to temperature changes. First, the dye is generally loaded onto the outer surface of the particle which means that it will begin to respond to changes in temperature

faster than the particle itself. Secondly, the photo-physical response of the dyes have an inherent response time which is not included in the heat model above. For these reasons, it was important to empirically measure the response times of the particles.

A method for measuring temperature time response was developed for liquid crystals by Ireland and Jones.[8,9] This device introduces as fast temperature change to a foil strip with a sample cured onto it. The sample then responds to the temperature change under observation. This device was the basis for a similar device developed by this research group to study the response times of various temperature-sensitive dyes. The device and methods used are discussed extensively in section 3.2.

2.4 Reference Dye and Spectrum Limitations

When using the intensity method for TSP, a reference image is required to account for irregularities in illumination, concentration, and other geometric anomalies. For TSP, this is most often a 'wind-off' image or other reference condition where the temperature is known. This works because the painted surfaces do not move, move very little, or move in a predictable manner. For PIV, a 'wind-off' condition is not possible as the particles are in motion while testing and it is not be possible to reconstruct the same flow field with the exact same particle placement at a reference temperature. Instead, a reference dye is used. In this case, a temperature insensitive dye is also used in conjunction with the temperature-sensitive dye. This reference dye is subject to the same concentration, illumination, and geometry anomalies that the temperature dye is subject to and thus can be used to account for the variance. Normally, the temperature intensity is ratioed with the reference intensity. This has been shown to work in paint based luminescent tests[32] and helps account for spatial variation in intensity measurement.

The limitation of this method is finding a temperature-insensitive dye (ie. reference dye) that will fit as a separate emission peak within the spectral limitations of the cameras and excitation source. Both the temperature and reference dyes need to

be excitable by the same excitation source and must emit at distinguishable wavelengths, ideally with no spectral overlap. One other consideration for reference dye selection is whether both dyes can be equivalently loaded onto the particle. Not all combinations that theoretically work in terms of absorption and emission work on a practical level if one dye is much dimmer than the other or if, chemically, the loading of one dye prevents the loading of the other. The dyes must both have emission intensities on the same order of magnitude for practical use. The emission and absorption spectra of the dyes considered in this project can be found in Appendix A.

2.5 Particle Size and Density

For a particle to be suitable for PIV, it must be the appropriate size to not only provide suitable imaging but to also follow the flow through the turbulence. Therefore, it is important to have a particle that is large enough to be seen but also small enough to follow the flow. To do this, it is useful to understand the length scales of the turbulence and then pick that largest particle that will still follow the flow. The Stokes number of a particle is largely used to determine this characteristic. The Stokes number,

$$St = \frac{\tau_p U_\infty}{l} \ll 1, \tag{2.7}$$

is a unitless ratio of particle stopping distance to the characteristic length scale of the flow, where τ_p is the characteristic time constant of a particle, U_∞ is the flow speed, and l is the characteristic length scale of the flow. If the stokes number is less than 1, a particle will be able to come to a complete stop in the distance l. This means that any features in the flow that are larger than l will be seen clearly in the motion of the particles around it. Features much less than l in length will not effect the velocity of the particles before they have passed by and therefore will be difficult if not impossible to distinguish in the motion of the particles. If the characteristic length l is set to be the smallest possible eddy size in a turbulent flow, the Kolmogorov length scale η, then the stokes number equation gives the largest particle that can

follow and distinguish the smallest of eddies.

To do this, the particle response time τ_p is needed:

$$\tau_p = \frac{(\rho_p - \rho_f) d_p^2}{18 \mu_f}, \tag{2.8}$$

where ρ_p is the particle density, ρ_f is the fluid density, d_p is the particle diameter, and μ_f is the fluid dynamic viscosity. From this, it is clear that the most important factors in getting a particle to follow a flow are matching the particle density to the fluid density and keeping the size small.

Chapter 3

PARTICLE PRODUCTION AND CHARACTERIZING PARTICLE TEMPERATURE SENSITIVITY

The concept of temperature-sensitive microbeads had been proven previously by this lab.[24,31] Therefore, the primary concern with particle selection and use was actual particle performance. It was important to characterize the time response of the temperature particles to determine whether they would be suitable for various unsteady testing conditions. It was also important to balance this time response against the effectiveness of the particle as a temperature sensor. A fast responding particle that shows minimal intensity change with temperature and a very responsive particle that responds very slowly would both be poor candidates. It was necessary to find a particle that correctly balanced temperature response with an appropriate time response.

3.1 Particle Production

Particle production was an iterative process with much trial and recourse to approach a more ideal particle. Previous research had shown that successful particles could be produced in small quantities by outside laboratories[24,31] but at a high cost. These particles were visible as distinct particles under laser excitation and showed moderate success as sensors. However, they were characterized as slow responding which did not meet the criteria established for future turbulent analysis. They also relied on expensive production techniques that limited the use of the particles to small scale applications. For this reason, particle production focused primarily on producing faster responding particles, preserving particle brightness, and producing the particles with

Table 3.1: Particle Properties

Particle	Supplier	Material	D µm	ρ g/cm^3	τ_p us	τ_T µs
110P8	Potters	Spherical Glass Hollows	11.7	1.1	9.40	15.72
SiO2MS	Cospheric	Silica Microspheres	2-19	1.67	3.75	5.86
SH400S20	Potters	Silvered Hollows	13	1.6	16.88	24.36
SH230S33	Potters	Silvered Hollows	44	0.5	60.42	78.17
SH230S50	Potters	Silvered Hollows	45	0.6	75.84	83.32
Q-cel 6014	Potters	Hollow Microspheres	85	0.14	63.14	-
Glass Bubbles	3M	Glass Bubbles	65	0.16	42.20	70.59
Glass Bubbles	3M	Glass Bubbles	16	0.6	9.59	16.04
Ceramic Microspheres	3M	Ceramic Microspheres	4	1.5	1.50	-

readily available materials to save on cost. For most of the particle production, prefabricated particles were dyed in-house with luminescent dyes. A table of the particles used in-house can be seen in Table 3.1. This table includes the size, density, and response times to velocity and temperature step changes per the equations discussed in Sections 2.3 and 2.5.

3.1.1 Evaporation Method

The simplest method and often most effective method for making particles involved evaporating a dye carrying solvent while suspended substrate particles are mixed continuously in the solvent. Dye was chosen based off of tests described later in this chapter and inert particles were chosen for dying based on their diameter, density, surface geometry, and particle uniformity. For this procedure, 5 mg of dye would be dissolved in a 50 mL of solvent. The solution was poured into an evaporating flask and 500 mg of particles would be added to this solution. This mixture was then stirred continuously with a magnetic stir bar at room temperature until the solvent

had completely evaporated.

A variety of particles were tested as substrates for various dyes. As each particle required different concentrations of dye to optimize brightness, a small selection of similar particles were chosen and optimized for brightness and balanced loading between the dyes used. The primary substrate particle for this testing was the Potters Sphericel Hollow glass microspheres and the Potters Conduct-o-fil silver coated glass microspheres. These particles were available in large quantities, exhibited sufficient uniformity of shape, size, and density, and displayed favorable loading properties.

Different dyes required different solvents but primarily methanol, isopropanol, and methylene chloride were used. These three solvents provided a range of evaporation rates for varying results. The methylene chloride evaporated the fastest for the fastest production of particles but this introduced variation between particles in the same batch. The rapid evaporation of the solvent left some particles more loaded than others. Both methanol and isopropanol provided good results for reasonable evaporation rates. When left stirring for 12-24 hours the solvent would be completely evaporated and the particles would be ready for use with much more consistent loading than that provided by the methylene chloride. The advantage of this method is very heavy loading of dye onto the particles and good control over the known amount of dye that would be guaranteed to be loaded onto the particles. This method involves very few variables and is simple to optimize. The disadvantages of this method are potentially uneven loading on the particles in the same batch and a tendency for the particles to clump together once the solvent evaporates. These clumps would have to be broken up through sonication or grinding after production.

3.1.2 Refluxing Method

An adaptation to the evaporation method was made to try to ensure more consistent loading within a batch of particles. Rather than completely evaporating the solvent this method relied on refluxing the solvent to load the dye onto the particles. For

this, the same solution of dye and particles was instead poured into a boiling flask and placed in a sand bath over mild heat. The temperature of the solution was allowed to reach the boiling point of the solvent. A condenser placed above the boiling flask was then used to condense the solvent and return it to the flask. This process was allowed to cycle for various amounts of time until it was deemed that enough dye had been loaded onto the particles. It was found that this method does not produce particles of the same luminescent intensity as the evaporation method. The advantages of this method, however, were more uniform dye loading in the batch and the maintenance of the particles in the colloid solution. Because the particles remained in solution for this process, there were no issues with particles forming clumps or sticking together.

3.1.3 Bubble Template Method

A third method for making particles involved producing the particles from s polymer solution using microbubbles as templates to control particle size. This method is based off of a similar method for making pharmaceutical drug delivery systems.[38] For this method a 2% (w/w) poly(vinyl alcohol) (PVA) solution and a $2\,\mathrm{g\,L^{-1}}$ Poly(methyl methacrylate) (PMMA) methylene chloride solution were prepared. The PMMA solution was deposited into the PVA solution in droplets via a 5 µL syringe. The droplets of PMMA solution were limited to 5 µL in volume. The beaker was then placed in a pressure chamber and subjected to 3 atm air pressure for 1 hour. The beaker was then removed from pressure and let sit for 24 hours for the microbubbles to form and shed from the droplets. The particles were then collected and washed from the PVA solution and the remaining PMMA droplets discarded. This method has the potential to be much brighter and more uniform than the previous methods. The incorporation of the dye into the particle (rather than the application on the surface) may make the particles much brighter. The microbubble templates also allow for very uniform size control. The disadvantage of this method is developing a way to produce particles at a large enough scale to be useful for wind or water tunnel testing. The

number of particles produced by this laboratory was very limited at best and the bubble template particles were not able to be tested against the particles produced through the other methods.

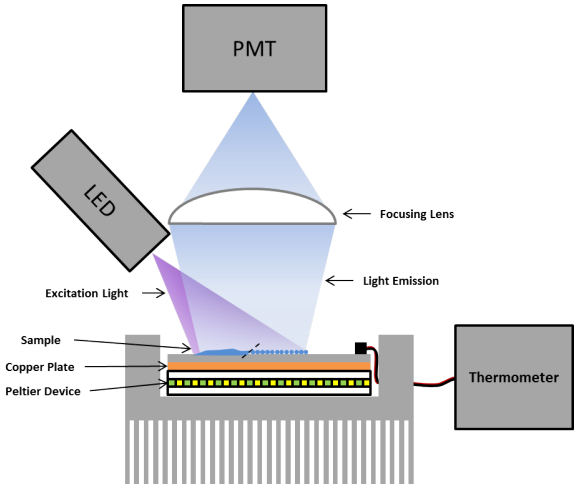

Figure 3.1: Temperature cell for testing changing emission of particles under varied temperature.

3.2 Particle Temperature Sensitivity

The first step for testing was to identify a series of candidate dyes that respond to changes in temperature with a corresponding emission change. The dyes that were available for testing are listed in Appendix A along with their absorption and emission spectra.

3.2.1 Device and Methodology

To test the response of the dyes to changes in temperature, a heated cell was constructed with a Peltier thermoelectric device attached to a heat sink and a copper plate. A drawing of the device can be seen in Figure 3.1. Depending on the direction of electrical current applied to the device, the cell could be heated or cooled. The dyed sample was then placed on the copper plate with thermal paste (Omegatherm 201) along with a thermocouple for measuring the temperature of the plate.

The dyed sample consisted either of a dyed particle layer or of a dyed polymer film. Initially, a dyed film was tested to determine dye properties then later dyed particles were tested to ensure they maintained the characteristics of the constituent

dyes. Temperature was controlled by varying the voltage and current applied to the Peltier device and then waiting 5 minutes for the temperature to reach a new stable equilibrium. The samples were excited under 365nm LED light and the emission was then focused and captured in a photo-multiplying tube and/or a spectrometer.

Band-pass filters were used on the photo-multiplying tube to isolate the intensity at different bands of the spectrum for each dye. Filters were carefully selected to isolate the individual dyes. The change in intensity for each dye was recorded for a range of temperatures from room temperature up to more than 40 degrees C. With the spectrometer, multiple spectral images of each sample were taken at each temperature to average out any noise. The multiple spectra at each temperature were averaged together and then plotted. These spectra can be seen in Figure 3.2. Using numerical integration, intensity values for these peaks were found and then plotted against the temperature recorded for each spectrum. Integration limits were chosen for each dye independently based on an appropriate band-pass filter for viewing each dye. These limits can be found in Table 3.2. This results in a linear trend or intensity decreasing as the temperature increases. Lines for the dyes tested are plotted in Figure 3.3.

Comparing the slopes of these lines for different dyes gave an indication of which dyes responded with the most pronounced intensity change to a change in temperature. The percent change per degree Celsius for the primary dyes tested can be seen in Table. 3.3. Figure 3.4 shows the spectra of a 13 µm spherical glass hollow coated with both E and G dyes at a series of different temperatures. The primary temperature-sensitive peak of the E dye can be seen at 615 nm. Clearly visible in the spectra, E dye diminishes in intensity with an increase in temperature due to thermal quenching. This trend is visible in Figure 3.5.

3.2.2 Results

E dye showed a marked advantage over the other dyes in terms of temperature sensitivity. Other candidates included F dye, R dye, and C dye due to their temperature

Table 3.2: Bandpass Limits for Dye Intensity Measurements

Dye	Bandpass Wavelength	Bandpass Width
E	615 nm	30 nm
F	625 nm	100 nm
R	625 nm	100 nm
ZnO	575 nm	100 nm
C	625 nm	100 nm
D	525 nm	100 nm

Table 3.3: Dye and Luminophore Temperature Sensitivity

Dye	Full Name	%/°C	R^2
E	Europium (III) thenoyltrifluoroacetonate	−2.90	0.996
F	Rhodamine base B	−1.76	0.999
R	tris-(Bathophenanthroline) Ruthenium (II) Chloride	−1.51	0.996
ZnO	Zinc Oxide	0.511	0.980
C	Ir(mebtp)3	−2.02	0.993
D	Bis(3,5-difluoro-2-(2-pyridyl)phenyl-(2-carboxypyridyl)iridium III	−0.76	0.987

Figure 3.2: Emission Spectra of Various Temperature Sensitive Dyes Tested

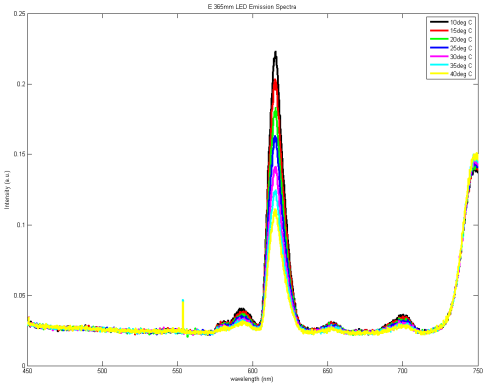

(a) E Dye Spectrum

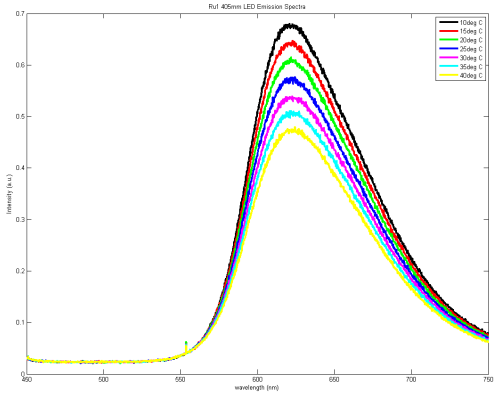

(b) R Dye Spectrum

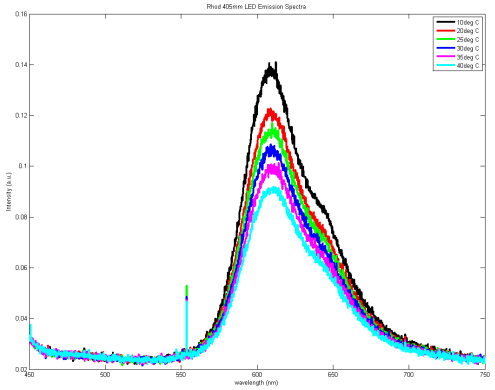

(c) F Dye Spectrum

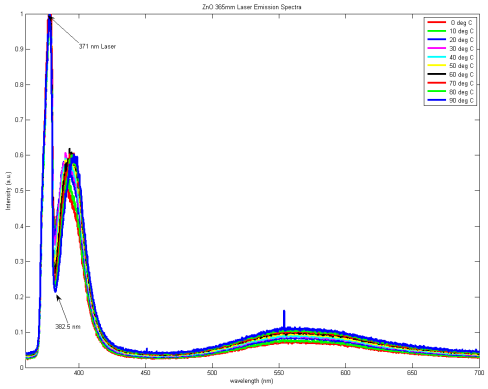

(d) Zinc Oxide Spectrum

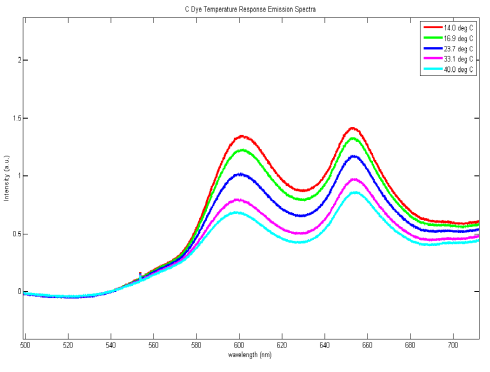

(e) C Dye Spectrum

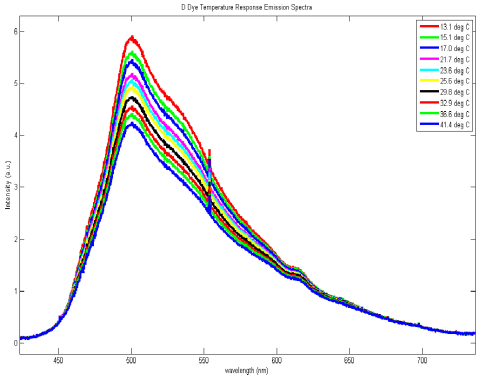

(f) D Dye Spectrum

Figure 3.3: Temperature Sensitivity of Various Temperature Sensitive Dyes Tested

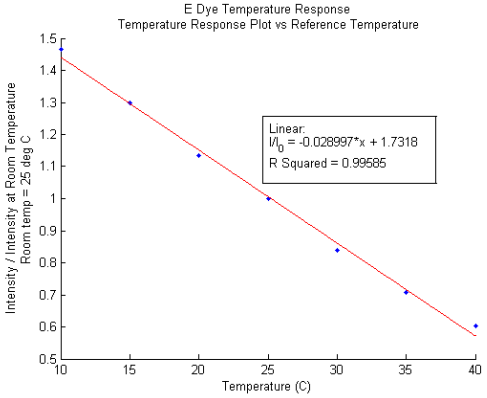

(a) E Dye Temperature Sensitivity

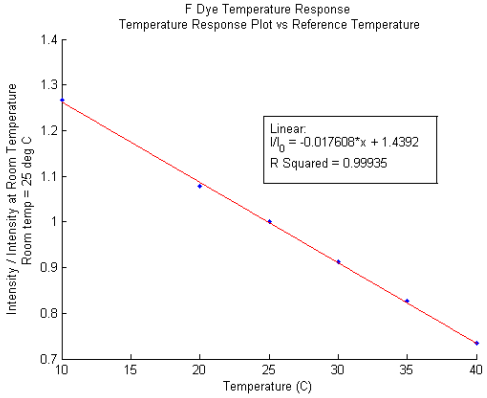

(b) F Dye Temperature Sensitivity

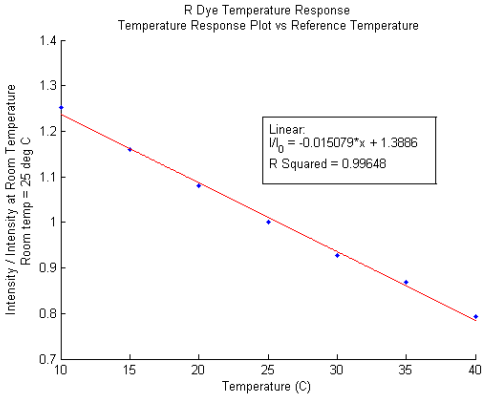

(c) R Dye Temperature Sensitivity

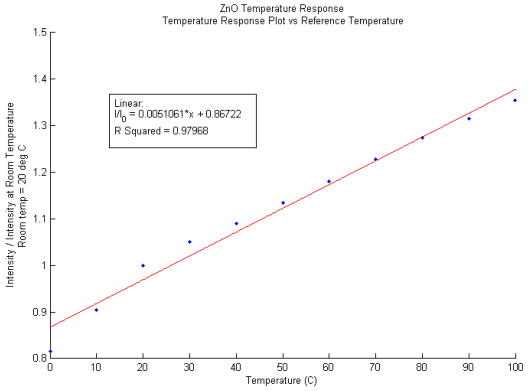

(d) Zinc Oxide Temperature Sensitivity

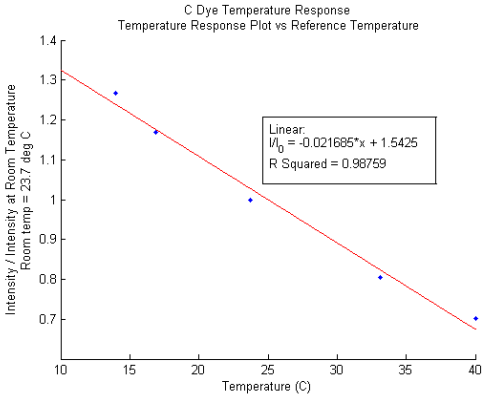

(e) C Dye Temperature Sensitivity

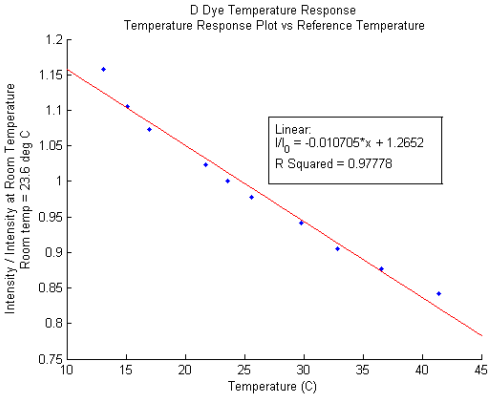

(f) D Dye Temperature Sensitivity

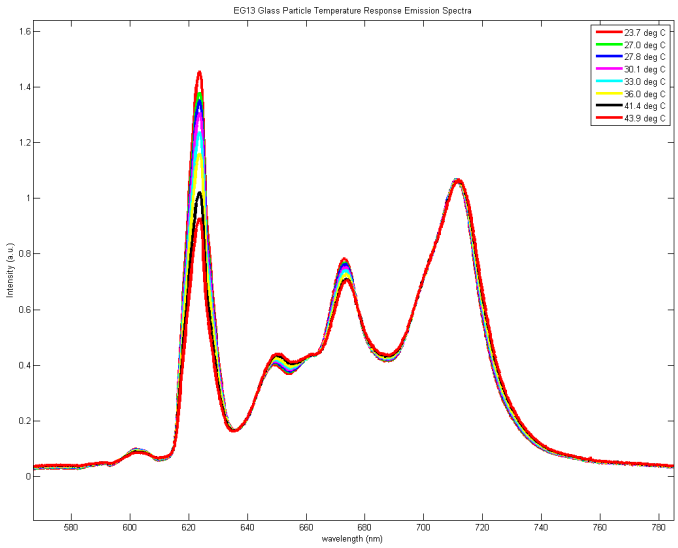

Figure 3.4: Spectrum of dyed hollow glass particles with both temperature and reference dyes. E dye peak at 620nm is sensitive to temperature changes while G dye peak at 710nm is not. Peaks in between are secondary peaks from the 2 dyes and are thus filtered out due to their overlapping behaviors.

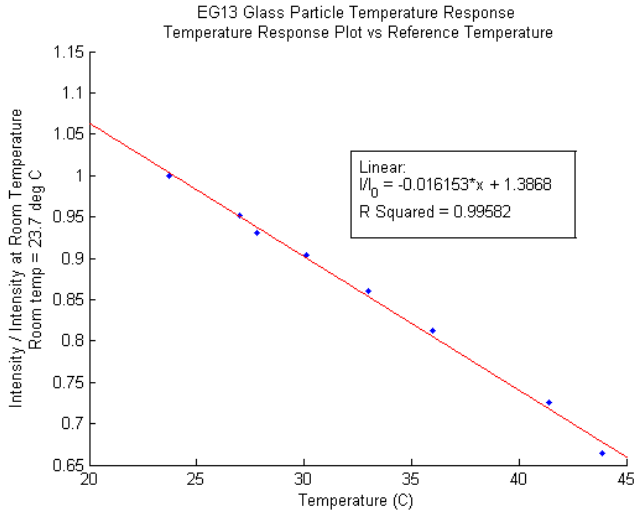

Figure 3.5: EG coated 13 micron spherical glass hollow temperature sensitivity.

sensitivities. Other factors, such as emission intensity, solubility, and oxygen sensitivity also had to be considered when choosing an appropriate dye. F dye is soluble in water which means it cannot be used in water tunnel experiments. R dye and C dye are oxygen sensitive, necessitating use in a water tunnel or another oxygen-free environment for consistent temperature measurement. E dye is the most versatile of the candidate dyes as it is suitable for both water applications and air applications.

Chapter 4

DEVICE AND METHOD FOR TEMPERATURE RESPONSE TIME EVALUATION

Temperature time response is an important consideration when addressing a system's merit in measuring unsteady phenomena. The time it takes a measurement system to respond to and correctly read a temperature change plays a role in which flows it can measure. It is not suitable for a device to be only accurate; it must also display the correct temperature that is associated with the time of the reading. A delay of several milliseconds can mean that the temperature is recording the wrong part of a passing turbulent eddy. For this reason, it was important to measure the response time to temperature changes of the various dyes used in the production of the temperature-sensitive particles. This would allow the selection of a suitable dye and prevent the selection of a dye that exhibits too slow a response.

4.1 Device Setup

To test the dye and particle response time to changes in temperature, a device was developed to generate a sharp temperature rise in the luminescent sample. The device was developed by Roy Olund of the UW Chemistry Electronics Shop based off of a similar device used by Ireland and Jones.[8] The device utilizes energy storage capacitors, a heating element and a fast switch. It also incorporates a voltage sensor and current sensor through the heating element with scaling amplifiers for the outputs. The heating element consists of a thin strip of titanium held between copper pylons. The wiring is such that this strip acts as a four terminal load resistor. This is setup such that both current and voltage can be read through the titanium strip. Titanium

was chosen due to it's high heating rate under current. For the same voltage and current, titanium accumulates heat at a much faster rate than more common metals. To determine the rate of heating, the temperature rise is written,[8]

$$\frac{dT}{dt} = \frac{I^2 r}{A^2 \rho C_p}, \tag{4.1}$$

where I,r,A,ρ, and C_p are the current, resistivity, cross sectional area, density, and specific heat capacity of the foil respectfully. A heating merit quantity can be defined as $K_H = \frac{r}{\rho C_p}$ to compare different metals heating rates for the same current and cross sectional area. A list of heating merits can be found in table 4.1. It is clear that titanium and zirconium are the optimum metals for heating speed. Titanium is available more readily as a foil and was therefore chosen for this device.

The gate in the circuit can support up to 12 A of current and the capacitors were generally charged to 35-50V. Different voltages could be set to vary the amplitude of the temperature change. The capacitors rapidly discharge and heat the titanium foil when the circuit is closed by the pulse driven fast switch. Pulse durations of 40 µs to 250 µs were used to create rapid temperature rises in the titanium strip.

4.2 Methodology

On the titanium strip, a small sample of dyed film or particles was placed in a thin layer. It was assumed that the thermal mass of the samples are insignificant during heating but it is still essential to have a uniformly thin sample so that there is no depth of response from heat transfer delays through the sample. For this reason, particular care was used to make the films as thin and consistent as possible and for the particles to be deposited in a monolayer or sub-monolayer such that all particles have a similar contact with the titanium strip. For the dye comparison, samples consisted of 2.5 µL of a dye solution dropped on the titanium foil and let to evaporate. The dye solution consisted of 8mL of 1% polycarbonate in dichloromethane with 250 µL of a 2.5 mg mL^{-1} stock dye added.

Table 4.1: Metal Heating Merit Comparison

Metal	Resistivity - r $\mu\Omega\,\mathrm{cm}$	Temp Coeff of R $\Omega\,^{\circ}\mathrm{C}^{-1}$	ρ $\mathrm{kg\,m^{-3}}$	C_p $\mathrm{J\,K^{-1}\,kg^{-1}}$	K_H
Aluminum	2.67	0.0045	2700	900	1.1
Beryllium	3.3	0.009	1848	1825	0.98
Chromium	13.2	0.00214	7100	518	3.59
Cobalt	6.34	0.0066	8900	456	1.56
Copper	1.69	0.0043	8960	385	0.49
Gold	2.2	0.004	19300	129	0.88
Indium	8.8	0.0052	7300	234	5.15
Iridium	5.1	0.0045	22400	133	1.71
Iron	10.1	0.0065	7870	444	2.89
Molybdenum	5.7	0.00435	10220	251	2.22
Nickel	6.9	0.0068	8900	444	1.75
Palladium	10.8	0.0042	12000	244	3.69
Platinum	10.58	0.00392	21450	133	3.71
Silver	1.63	0.0041	10500	237	0.66
Tantalum	13.5	0.0035	16600	140	5.81
Tin	12.6	0.0046	7280	213	8.13
Titanium	54	0.0038	4500	523	22.94
Tungsten	5.4	0.0048	19300	133	2.1
Zinc	5.96	0.0042	7140	388	2.15
Zirconium	44	0.0044	6490	281	24.13
Stainless Shim	21	0.0013	7800	500	5.38

Temperature was determined for the titanium by computing the resistance as a function of time. Using a fast data acquisition system (NI USB-6251) it was possible to record both the current and voltage for the titanium foil. From these the resistance was calculated. The temperature change was then found using the temperature coefficient of resistance of the titanium strip. This allows for the temperature to be plotted in the time domain.

The sample was excited with a 365 nm LED light source and recorded with a photo-multiplying tube (PMT). The voltage from the PMT was read into the data acquisition system along with the current and voltage from the circuit board. Data acquisition occurred at a rate of 400 kHz for 2.5 µs data ticks. These three signals form the basis for the time response analysis.

The signal data was aligned and mapped on the time domain. The PMT voltage was generalized as an intensity value ($\mathcal{I}$) with arbitrary units*. This signal was first detrended throughout based on the room temperature region before the temperature pulse and then normalized against the room temperature intensity ($\mathcal{I}_o$). Once normalized, the intensity ratio was converted to a temperature value,

$$\frac{\frac{\mathcal{I}}{\mathcal{I}_o} - 1}{m} = T - T_o, \tag{4.2}$$

where m is the slope of the steady-state temperature sensitivity found in section 3.2 and T_o is room temperature. The temperature in the titanium strip is found by relating the temperature coefficient of resistivity to the resistance found in the titanium strip over time. Resistance was calculated from the recorded current and voltage:

$$R = \frac{V}{I} \tag{4.3}$$

*The standard unit for luminescent intensity is the candela but here intensity unit is arbitrary as it is ratioed out with respect to temperature.

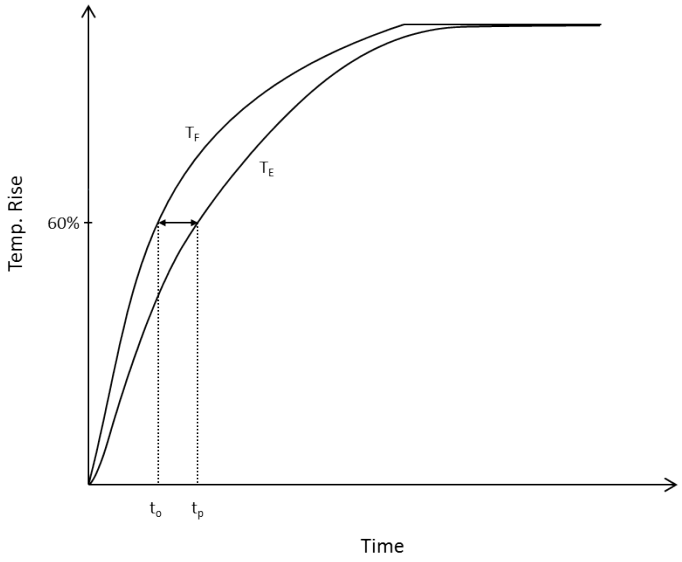

Figure 4.1: Temperature Time Response Example

The resistance is then used to calculate the change in temperature in the titanium.

$$\frac{R - R_o}{\frac{dR}{dT}} = T - T_o \tag{4.4}$$

These temperature changes were normalized from 0-100% change and mapped against each other for easier comparison. This test was repeated for each dye 10-12 times to achieve an average time response. Time response was measured as the time difference between the incident temperature change of the titanium strip and the response temperature measurement of the luminescence at 60% of the total change. An example of this can be seen in Figure 4.1. T_F is the temperature of the titanium foil and T_E is the temperature measured from the emission. t_o is when the foil reaches 60% of the and t_p is when the emission records the same change. The temperature time response is the difference between t_p and t_o.

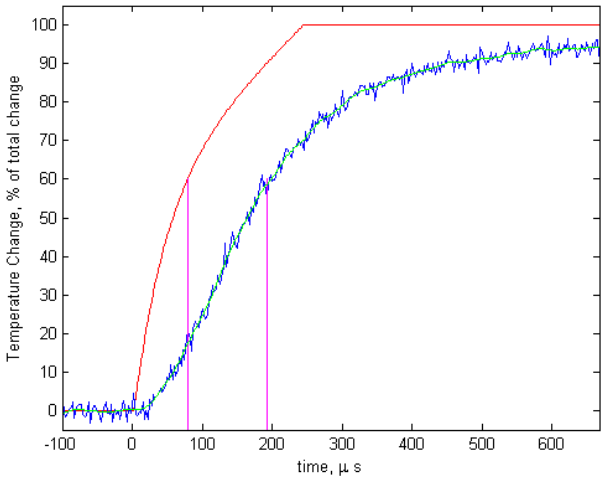

Figure 4.2: Temperature Time Response of E Dye. The red line shows the temperature rise in the titanium as measured by the resistance in the circuit. The blue line shows the temperature rise of the emission after conversion with the stead-state temperature sensitivity. The vertical magenta lines denote where each line crosses the 60% temperature change threshold.

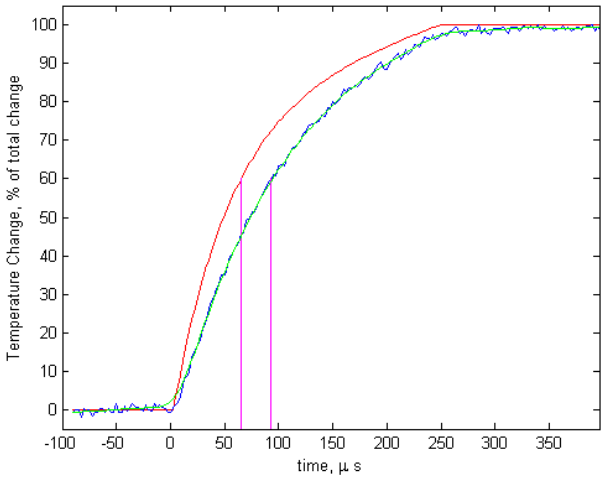

Figure 4.3: Temperature Time Response of R Dye. The red line shows the temperature rise in the titanium as measured by the resistance in the circuit. The blue line shows the temperature rise of the emission after conversion with the stead-state temperature sensitivity. The vertical magenta lines denote where each line crosses the 60% temperature change threshold.

4.3 Results

Select plots of the temperature response time of E dye and R dye can be seen in Figure 4.2 and Figure 4.3 respectfully. The results from this experimentation are summarized in Table 4.2 for all 3 dyes. As expected, the fluorescent R and F dyes were faster than the phosphorescent E dye. Unexpectedly, R dye showed a faster response time and F dye. R dye has a luminescent lifetime of approximately 10 µs[39] while F dye has a lifetime of approximately 2.9 ns.[40] This disparity could be an effect of the polymer thickness. While the volume and mass of the sample could be precisely controlled, the drying thickness of the samples was subject to the evaporative process with which they were applied to the titanium. During this process, there may be been some variance which caused the F dye to have a thicker polyer film. The film thicknesses were not measured, however, and this is can only be considered conjecture. Statistically, the standard deviations of the 2 dyes intersect, therefore it may have been sampling which resulted in the response of the F dye appearing longer than that of the R dye. More tests were conducted with the same solutions, however, and the trend remained.

If choosing a dye for only temperature response time, the choice would be between F dye or R dye, however, many other factors also play an important role in dye selection. Several problems with the two faster dyes meant that E dye was the best candidate for a particle dye. F dye, while temperature-sensitive, is very soluble in water. This limitation would prevent the use of any particles made with F dye in a water tunnel. At this point in the research, a water tunnel application was deemed necessary and F dye was temporarily removed from the candidate list. While a water tunnel experiment was the short term goal, eventual wind tunnel experiments would limit the eventual use of an R dye particle as it is also highly oxygen sensitive. E dye, which is usable in both wind and water applications was deemed the best first candidate for particle testing.

Table 4.2: Dye Temperature Response Time

Dye	λ_i	λ_e	Average Time Response	STD
E	365 nm	610 nm	136.6 µs	20.1 µs
F	532 nm	580 nm	49.3 µs	13.8 µs
R	365 nm	580 nm	27.6 µs	9.4 µs

Based off of these results, subsequent particles were produced with E dye and G dye on hollow glass microsphere substrates using the evaporation technique described previously. Once optimized these particles displayed sufficient temperature sensitivity and an a short enough time response for many turbulent applications.

4.4 Further Applications of Device

The testing with this device showed additional applications of the device. It was clear from testing that the dye choice was not the only variable in determining response time. Thickness, mass, and polymer choice all seemed to also effect the response time. For these test, these variables were kept consistent across all dye samples to test teh effect of changing the dye. Future testing could be conducted where the device is used to test the effect on response time of various polymers or of the thickness of the sample. This could be used to quantify the time response of commercially available temperature-sensitive paints when applied with a different number of coats or primer layers. The application of this device has potential to help advance not only temperature-sensitive particles but temperature-sensitive paints as well.

Chapter 5
SOFTWARE DEVELOPMENT

To fully process the images taken for experimentation a series of software codes had to be developed that could both properly process the data and run efficiently. These codes were developed such that they could be implemented as functions in an overall work flow. They are fully commented and were written to be simple to use for future graduate students in their own work flows. The basic image processing work flow for the 2-D images take can be seen in Figure 5.1. This work flow involves a flat-field correction, averaging of a number of images to reduce noise, spatial image registration and interpolation, as well as the final ratioing of the images. The following sections will address each of the major processes and their implementation.

5.1 Flat-Field Correction

Flat-field correction is necessary in any image data set to account for various non-uniformity issues across an image. The main four main issues it accounts for are relative intensity variation due to the lens, non-uniform pixel sensitivity, background subtraction, and ambient light subtraction. Relative intensity variations occur in almost all imaging systems and are seen as a difference in intensity spatially across an image even when viewing a perfectly flat field. Primarily, this variation is attributed to light beams not following the central optical path of the lens being dimmed as an effect of the lens optics. This results in the edges and corners of images being dimmer than expected. The solution involves taking an image of a 'flat-field' or a uniform light distribution with the camera/lens setup and then accounting for the variation seen in this flat image in all future images. This process also helps account for slight

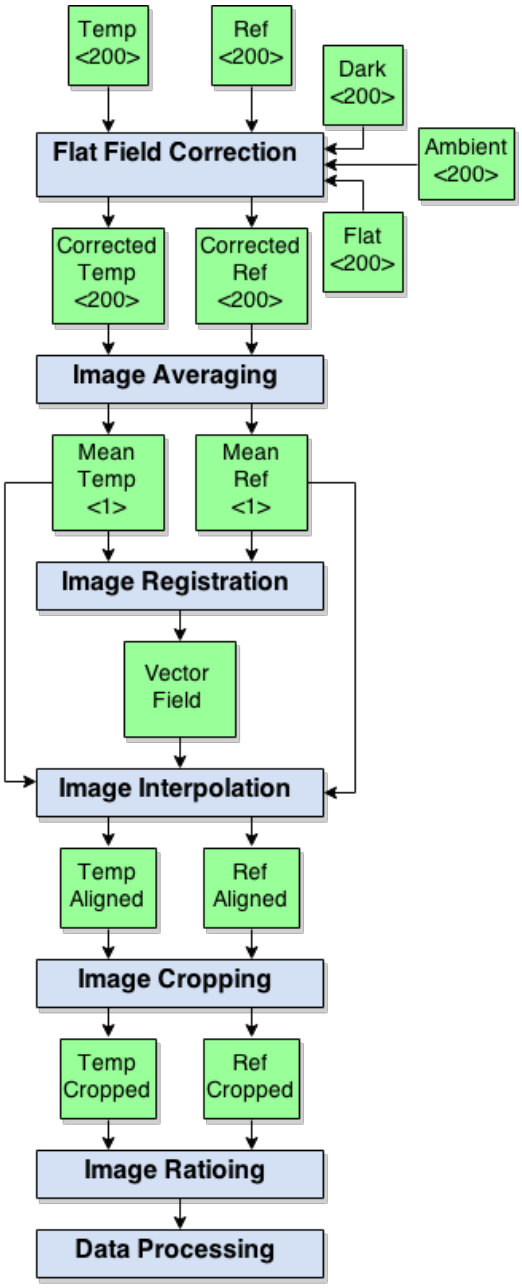

Figure 5.1: Basic image processing work flow. Green items represent images and data. Blue items are processes or functions applied to the data. Bracketed numbers $< \# >$ represent the number of images present in the data; these are dropped for succinctness after image averaging.

variations in individual pixel sensitivity. This image is called the 'Flat'.

The flat-field correction process, conveniently, can be mathematically combined with two other processes as they fit cleanly into the function. In order to properly apply a flat-field correction, a basis must be formed for the zero light condition as well. This image is generally taken with the lens cap left on and represents the background noise of the camera system. This image is called the 'Dark'. As it is already included in the function for flat-field correction, it is convenient to apply the background subtraction at this step as well. In fact, if an ambient light image is taken as well. It can be substituted in place of the dark (as it includes the dark background noise as well) in this subtraction. This results in a fairly simple mathematical function that accounts for all four the the previously mentioned variations in a single processing step. This function can be represented by the following equation for the flat-field corrected image, I_{FF},

$$I_{FF} = \frac{I - A}{F - D} M \tag{5.1}$$

where I is the raw image being corrected, A is the ambient light image, F is the flat-field image, and D is the dark image. M is a modifier added to scale the number back up to the range of values seen in the original image rather than leaving them as small values near 1. M is defined as,

$$M = mean(F - D). \tag{5.2}$$

The code developed for this process requires the raw data image as well as the flat, dark, and ambient images. This then out puts the flat-field corrected image per equation 5.1.

5.2 Image Registration

Image registration is the process of aligning two or more images so that the information contained in each images can be related. Even the most carefully aligned cameras will still have slight mis-alignments that need to be accounted for in the software. This

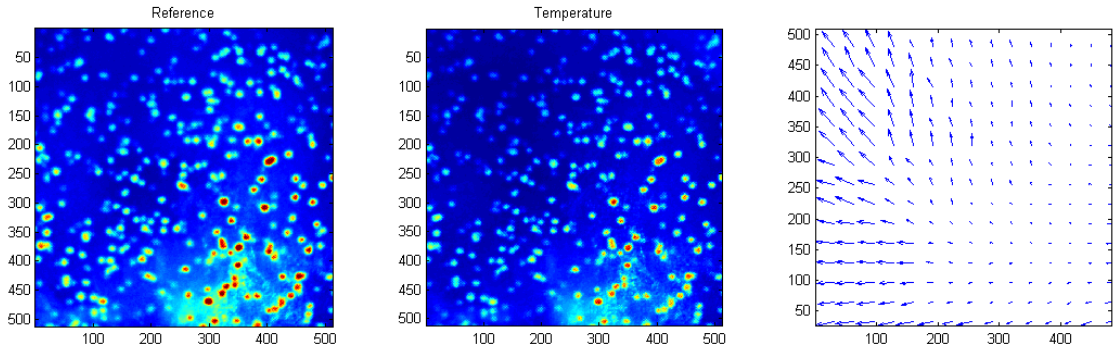

Figure 5.2: Image Registration Example with two particle images and vector field.

implementation of image registration utilizes a windowed cross-correlation that determines the vector displacement necessary to line up two particle image fields. The images are broken into smaller windows which are then subsequently cross-correlated. This cross-correlation yields the displacement necessary for each window. In this application, a two pass system is used such that a larger window first determines the coarse vector displacement and then a series of smaller windows are used to refine the vector field. This is referred to as multi-pass processing and is common in many PIV codes.

The code was developed for use in the processing work flow and this takes in the two images to be aligned and a series of various other arguments that control the alignment such as window size, overlap, and masking. It also allows the user to manually remove outlier vectors from the vector field generated.

5.3 Image Interpolation

Image interpolation utilizes the vector field generated by the image registration to then adjust one of the images to better match the alignment of the other. This process uses interpolation to find the adjusted pixel intensities based on the vector offsets found previously. A cubic interpolation is used, though this can be modified

to use any interpolation scheme, to find the sub-pixel intensity values at the locations that correlate to the pixel locations in the other image. This creates a new image that is in perfect alignment with the base image used for registration. In simpler words, it shifts each pixel in one image so that features line up in both images. Cubic interpolation is used because it provides a sufficient interpolation while reducing run time on the interpolation. More advanced interpolation methods are possible at the expense of computer resources, however, Park and Sung showed that for the added computational time often did not result in lower error.[41]

The code utilizes the outputs of the Image Registration code discussed in the previous section. It then interpolates the sparse vector field to every pixel in the image with a cubic surface interpolation. The newly found vector displacements of each pixel are then used to interpolate for new pixel values at the proper locations. Finally, the code outputs the new, shifted image.

Chapter 6

2-DIMENSIONAL FILM AND STATIONARY PARTICLE STUDIES

6.1 Optical Setup

The next test for the particles involved imaging them with cameras to determine their spatial consistency and imaging qualities. This involved developing an optical system such that two cameras could be set up to view the same particle field from the same direction through a series of filters and mirrors. This was necessary so that a third camera could at some point be positioned on the opposite side of the subject for 3-dye applications. Two Hamamatsu ImagEM X2 EMCCD cameras were used. These cameras have a resolution of 512x512 pixels and support 16-bit intensity readings allowing for 2^{16} different potential intensity readings. These cameras were chosen for their intensity sensitivity and the 16-bit capacity. This allowed for highly sensitive intensity measurements to be made.

The cameras were positioned and aligned through a dichroic mirror optical system designed for this application. The optical setup consists of 4 lenses set up in a relay with a dichroic cutoff filter positioned in the infinity-space to split the image between the two wavelengths. This setup can be seen in Figure 6.1 and Figure 6.2. The Edmund Optics 35mm F1.4, 1" Format front lens captures the image which is collimated by an identical relay lens positioned in reverse at twice the flange-back distance. The infinity focused beam is passed through a cutoff/long-pass filter to block the laser light from the cameras. A 532nm cutoff filter from Edmund Optics was used to eliminate reflected laser light from the images. For EG particles, the beam is then split by a Shemrock 662nm edge BrightLine single-edge imaging-flat dichroic

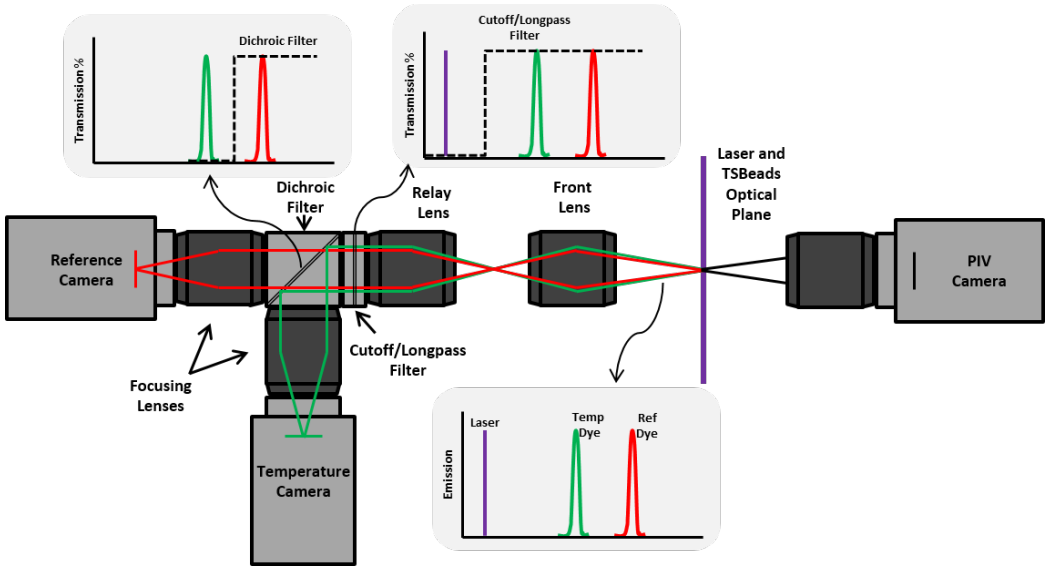

Figure 6.1: Experimental Setup with temperature, reference, and PIV cameras.

beamsplitter. Finally, the two beams are each refocused into the cameras by Edmund Optics 50mm F1.4, 1" Format lenses. The disparity between the lens focal lengths was to introduce a slight magnification to reduce the effect of relative intensity in the series of lens and to minimize vignetting.

The 1" format lenses performed best in our tests to provide a flat intensity distribution across the image under uniform illumination. Smaller format lenses tended to show significant falloff in intensity towards the edges and corners of the images. These lenses in particular were chosen based off of our testing for lenses with very flat relative intensity fields to provide the best initial images before flat-field correction. Figure 6.3 shows a comparison of a relatively bad flat-field image taken through three lenses to the improved flat-field taken through the three lenses chosen for the optical setup.

Figure 6.2: Lens assembly with 35mm lens, 35mm relay lens, dichroic beamsplitter, and 50mm refocusing lenses. Component drawings courtesy of Edmund Optics and Thor Labs

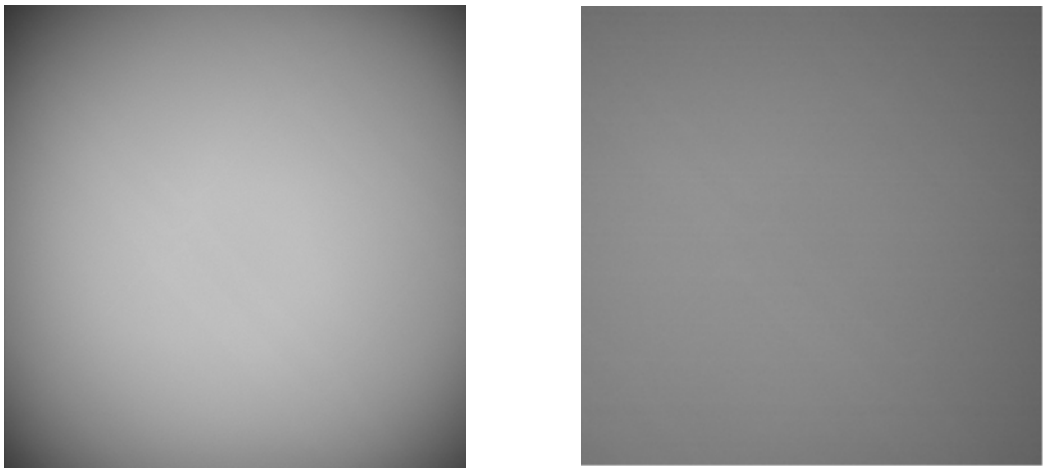

Figure 6.3: Flat-field comparison of different lenses setup in a 3 lens relay. The left image shows a flat-field taken through 3 sub-optimal lenses and the right image shows the flat-field taken through the 3 lenses chosen for the optical setup.

6.2 Temperature Measurement with and without Wind-Off Referencing

6.2.1 Temperature Measurement with Wind-Off Referencing

As a test of the algorithms and devices used, a temperature-sensitive paint was produced from E and G dyes dissolved in a polymer solution. This solution was applied to an aluminum slide through spin coating. Spin coating was the best way found to produce a thin, uniform film on the polished metal surface. Even with spin coating, small spatial variations were still visible through emission as the film was thin enough that very small scratches resulted in significant proportional film thickness variation. This thickness variation led to variation in emission intensity. An assumption was made that this variation was akin to spatial variation seen in actual application and thus methods had to be developed to account for it and other spatial variations seen.

Other spatial variations seen were relative-intensity variations, ambient light, variation in laser excitation illumination, and film features. Relative-intensity and ambient light variations have already been discussed in the previous chapter and are accounted for in the flat-field correction.

The standard method of accounting for accounting for spatial variation in excitation light and for film variance is known as wind-off referencing. This method is well established and is used extensively in industry for stationary films.[2,32] This method involves referencing the local intensity against the local intensity at known, uniform conditions. In other words, the test intensity distribution is corrected with the intensity variation seen at a reference condition.

With this method of correction, the films showed very uniform temperature measurement capabilities as seen in Figure 6.4. The standard method for temperature-sensitive paint was achieved with the dual-dye film. Next, a similar film was made by spreading a near monolayer of dual-dye temperature-sensitive particles over an aluminum slide. Using wind-off referencing again, the particles produced a very good temperature-sensitive surface measurement as seen in Figure 6.5.

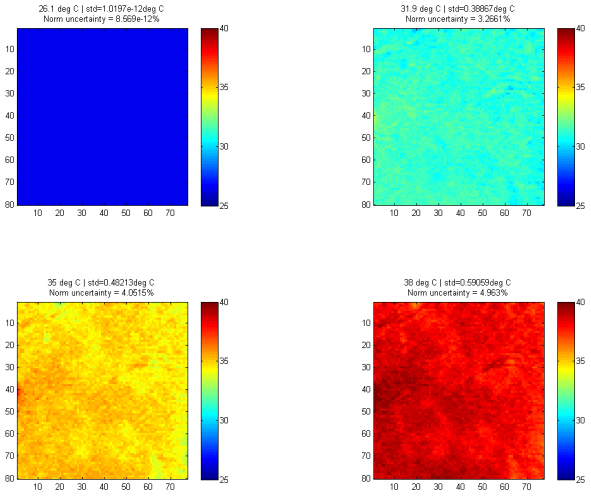

Figure 6.4: Classic Windoff Temperature Paint Result. Images were taken a series of temperatures and then normalized with the room temperature image.

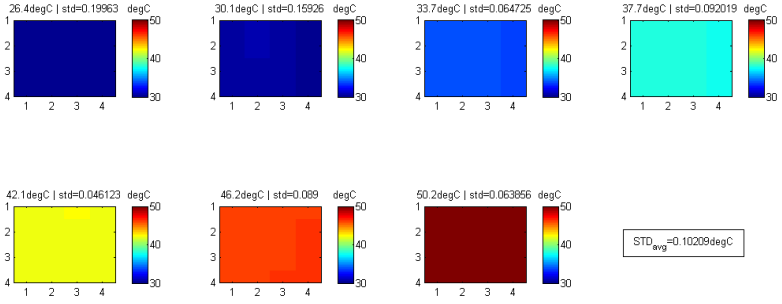

Figure 6.5: Classic Wind-off Temperature Particle Result. Images were taken a series of temperatures and then normalized with the room temperature image. 16x16 windowed averaging was used wchich resulted in a 7x7 gridded data.

With these two tests complete, the next step was to eliminate the wind-off referencing to determine the utility of the dual-dye particles in a non-stationary environment.

6.2.2 Temperature Measurement without Wind-Off Referencing

The same film data was analyzed without referencing to a wind-off reference case. In this case, the only the reference dye was expected to account for a large enough portion of the spatial variations to allow adequate temperature measurement. This single ratio (as opposed to the previous ratio-of-ratios) method can be seen in Figure 6.6. The results show that the ratio of temperature dye to reference dye does not account for all of the spatial variations seen in the intensity field.

The variation between the intensity distribution of the temperature dye and the reference dye is likely due to a difference in luminescent yield due to variations in excitation intensity between the two dyes. If the excitation energy is cut by 25% for both dyes, one might show a 30% drop in intensity and the other may show a 40% drop. After this test, it became clear that for a single ratio particle to succeed there needed to be another source of normalization to reduce the spatial variation. Another option would be to test the included dyes for their responses to change in excitation energy and then better match the dyes based on this new parameter. This becomes difficult when the limited selection of available dyes are considered and increasing more difficult when the other considerations discussed in Chapters 3 and 4.

To attempt to account for the continued problem of spatial variation, two methods were tested. The first involved added additional reference dyes to the film and particle samples to potentially allow for normalizing the reference spatial variation to that of the temperature dye. The second involved using a series of images taken of a non-stationary film and then temporally averaging the resulting ratio to give a synthesized 'wind-off' image for normalizing against.

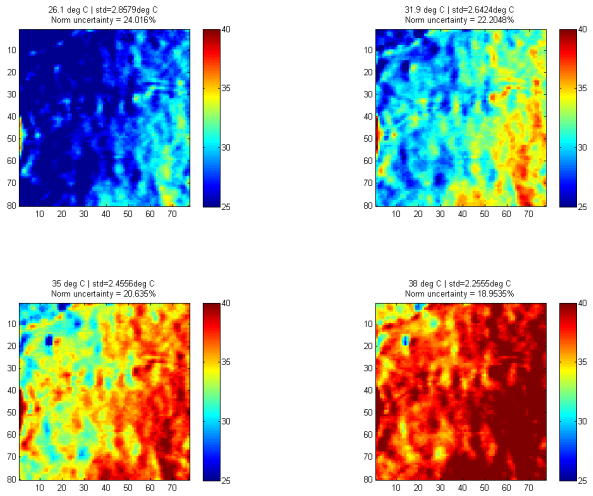

Figure 6.6: Single Ratio Temperature Paint Result. Images were taken a series of temperatures and then normalized with the room temperature image.

6.3 Quad-dye Attempt at Uncertainty Reduction

To reduce the spatial variation seen in the previous temperature measurements with no proper wind-off referencing, a film was produced that incorporated four separate luminescent dyes. These films were chosen such that all four would be excited by the same excitation light source and such that they each would emit at a unique wavelength each. These dyes were incorporated into a polymer film and applied to an aluminum surface for study in the experimental setup described earlier. The use of four dyes instead of two was tested to see if the addition of more reference dyes could account for the spatial variations in excitation energy and film/particle variances seen in previous the previous studies with no wind-off referencing. The addition of the extra dyes allowed for more reference points that could potentially account for some of the uncertainty that was not accounted for with the single reference dye. In this case, a pressure dye combination was used as it was much simpler to fit these 4

Table 6.1: Four Dyes for Quad-dye Pressure Sensitive Film

Dye	Full Name	Dye Type	Wavelength
K	Pt(II) meso-Tetra(pentafluorophenyl)phorpholactone	Pressure	740 nm
H	Coumarin 6	Reference	540 nm
G	meso-Tetra(pentafluorophenyl)phorphine	Reference	700 nm
J	Mg(II) meso-Tetra(pentafluorophenyl)phorphine	Reference	650 nm

dyes into the spectrum. A 4-dye temperature film and particle were also developed as these tests were being conducted. A spectrum 4-dye temperature-sensitive film can be seen in Figure 6.8.

This film consisted of the four dyes (K, G, H,& J) listed in Table 6.1. The excitation source for this experiment was a 2-dimensional bank of UV LED's filtered to a wavelength of 390nm. The emissions of the four dyes can be seen in Figure 6.7. From this spectrum, it can be seen that the pressure dye K can be referenced against the other 3 dyes to give an indication of pressure. This pressure dye was used in this case (as opposed to a temperature dye) as it was one of the few combination choices that allowed four separate dyes to fit within the spectral band. It was used to test the concept of using the four dyes to account for the spacial variations seen earlier.

The film was applied to an aluminum slide through spin coating to provide a very thin and uniform coating. This sample was imaged with a single camera through 4 separate band-pass filters at 535/10nm, 650/20nm, 700/15nm, and 750/15nm to isolate the individual dyes. A series of 100 images were taken through each filter and averaged to eliminate laser fluctuations and camera noise. Flat-field, dark field, and ambient light images were also taken through each filter. A dense particle field image was printed out on paper and positioned around the sample slide for image registration purposes. The sample images were flat-field corrected for flat-field, ambient light, and dark noise. The images were then registered and aligned to the 750nm image using

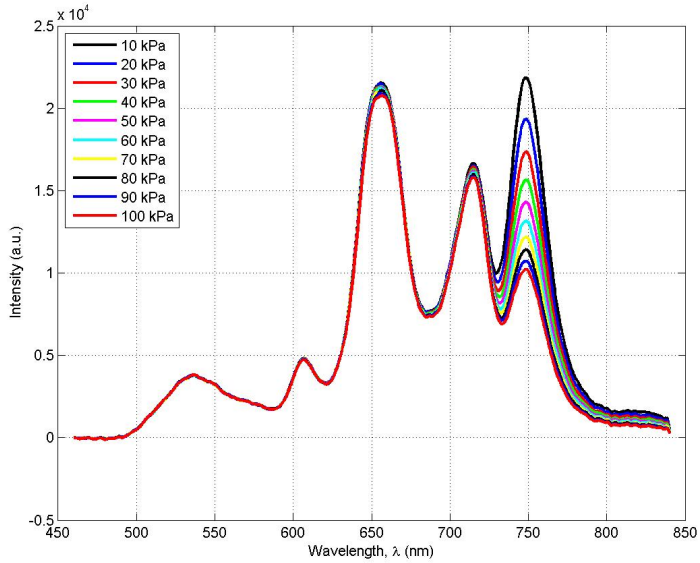

Figure 6.7: Emission spectrum and pressure response of the Quad-dye KGHJ film.

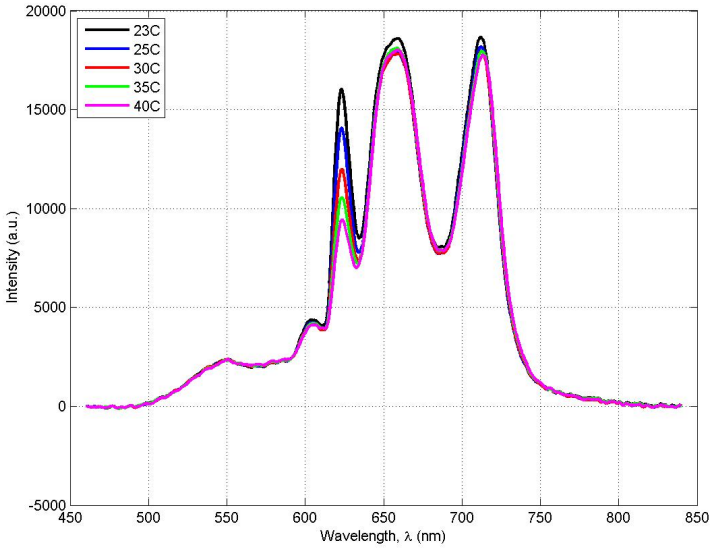

Figure 6.8: Emission spectrum and temperature response of the Quad-dye EGHJ film.

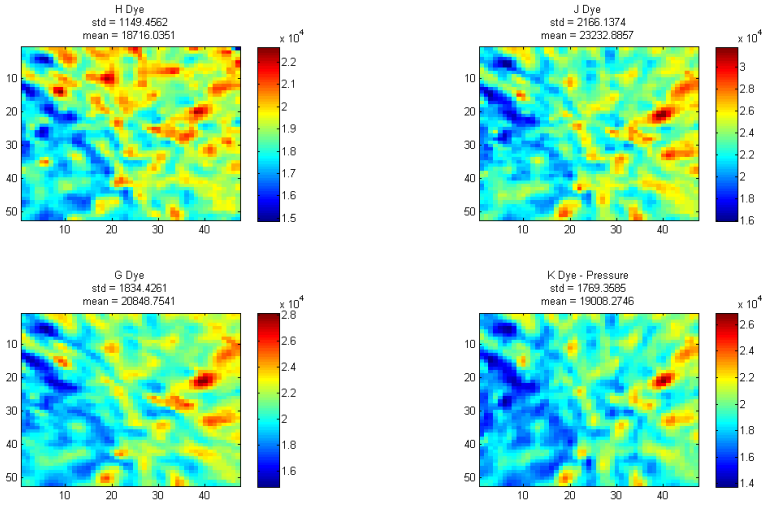

Figure 6.9: Individual images of the Quad-dye KGHJ film. Each image taken through a separate filter

a multipass PIV code applied to the particle field and image interpolation. The resulting, registered images can be seen in Figure 6.9. For all of these cases, the images were normalized against their mean so that the spatial variations would be easier to quantify in comparison to each other. To do this, each pixel intensity value of dye images was divided by the mean intensity value of the image. This resulted in images with mean intensities of 1 whose standard deviations were directly comparable.

Once aligned, the four dye images were used in various combinations to test various algorithms and methods for reducing the spatial variation seen in the dual-dye system. Initially, a ratio-of-ratios was produced where one ratio of two dyes was ratioed against another ratio of the remaining two dyes. In addition to this, various other dye fractions and mathematical operations, including averaging the reference set of images, were tried to reduce the spacial variations. The ratios-of-ratios and the more successful other methods can be seen in Figure 6.10. The normalized standard deviations shown are the standard deviation divided by the mean. These did not reduce the spatial

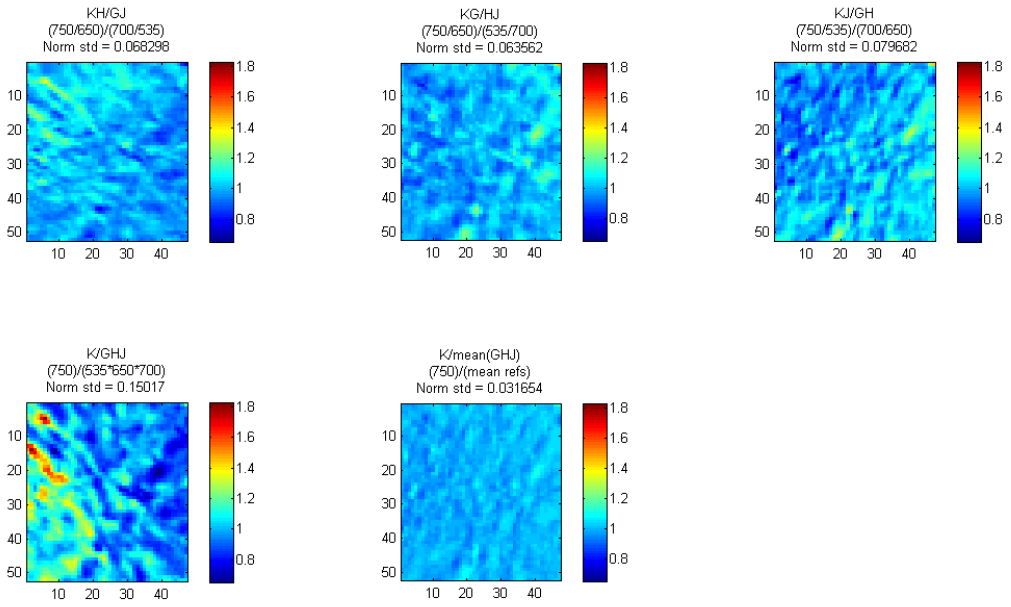

Figure 6.10: Ratio-of-ratios of the Quad-dye KGHJ film. Each image represents a different ratio or algorithm utilizing the 4 dyes.

variation beyond what a simpler dual-dye system could achieve. The most successful utilization of the quad-dye system was when the 3 reference dyes were averaged into a mean reference image and then ratioed against the pressure dye. In this case, however, the standard deviation was still not improved from that of a simpler single ratio. The spatial variation in the single ratios can be seen in Figure 6.11.

It was clear from these tests that the addition of the extra reference dyes did not add an additional reference with which to account for spatial variation.

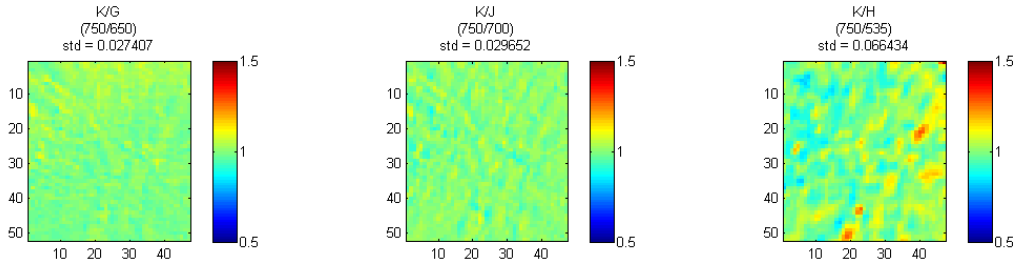

Figure 6.11: Single Ratios of the Quad-dye KGHJ film. Each image represents a different single ratio of the pressure dye to one of the reference dyes.

6.4 Substitute Referencing through Wind-Off Synthesis

6.4.1 Polymer Film Study

A new method for constructing a reference (or 'wind-off') image was formulated in an attempt to reduce the spatial variation through means possible in a moving particle wind tunnel application. While a typical wind-off image is not possible when the particles are moving a method to reduce the problem to that of an average particle was surmised. In this case, a reference image would be constructed through a time averaging of particle images passing through the laser field with no temperature variation or heat introduced to the test. In this way, a reference, or known temperature, condition would be found through a time averaged set of particle images. Through a convergence study, it would be possible to determine when enough of these particle images have been taken. This time averaged reference image would be a synthesized 'wind-off' image in that it would capture the spatial laser variation, which accounts for a large percentage of the spatial variation seen in the dual-dye system. Kose pointed our that one of the advantages of using a dual-dye luminescent system is that the wind-off, or reference images, no longer have to be perfectly registered and aligned to the test images.[32] It is this advantage of the dual-dye system which allows the use of a

looser definition of the reference image. It is important to note at this point, however, that while a traditional wind-off image accounts for variations in the film thickness, concentration, etc., this new reference image does not account for variations in the sample itself and only captures laser excitation variation.

To test this idea, a film study was conducted with an dual-dye film on an aluminum slide. The dual camera set-up introduced earlier was utilized with dyes E (EuTTA) and G (meso-Tetra(pentafluorophenyl)phorphine). A Shemrock 662 nm dichroic beam splitter split the wavelengths of the two dyes to the two Hamamatsu EM-CCD cameras. At room temperature, the film was imaged 25 times with slight movements of the film introduced between each image pair. Movements consisted of random translations and rotations such that each image showed a different piece of film for each pixel. It was not deemed necessary to use a new film for each of these image pairs as long as a sufficient assortment of orientations and translations were present to be able to average out any film details. This set of images will be refereed to as the reference set. Once this set of images were taken, a series of images were taken at 4 different temperatures (test set) as well as the necessary flat-field correction and image registration and alignment images. The images were all processed and then cropped to remove the background and only show the film.

The reference set of images were flat-field corrected and registered as per the normal order of operations. Then the set was averaged with a trimmed mean which neglected the top and bottom 10% of intensity values for each pixel. This resulted in an image which encompassed the change in ratio spatially with respect to the laser excitation spatial variation. The averaged reference set can be seen in the 2nd image of Figure 6.12. This represents a ratio correction parameter that needs to be applied to the recorded values in order to achieve a flat-field. The first and third images represent the room temperature ratio before and after the new reference image was applied. While the single ratio already accounts for much of the spatial excitation variation, the averaged reference image here shows that there is still spatial variation

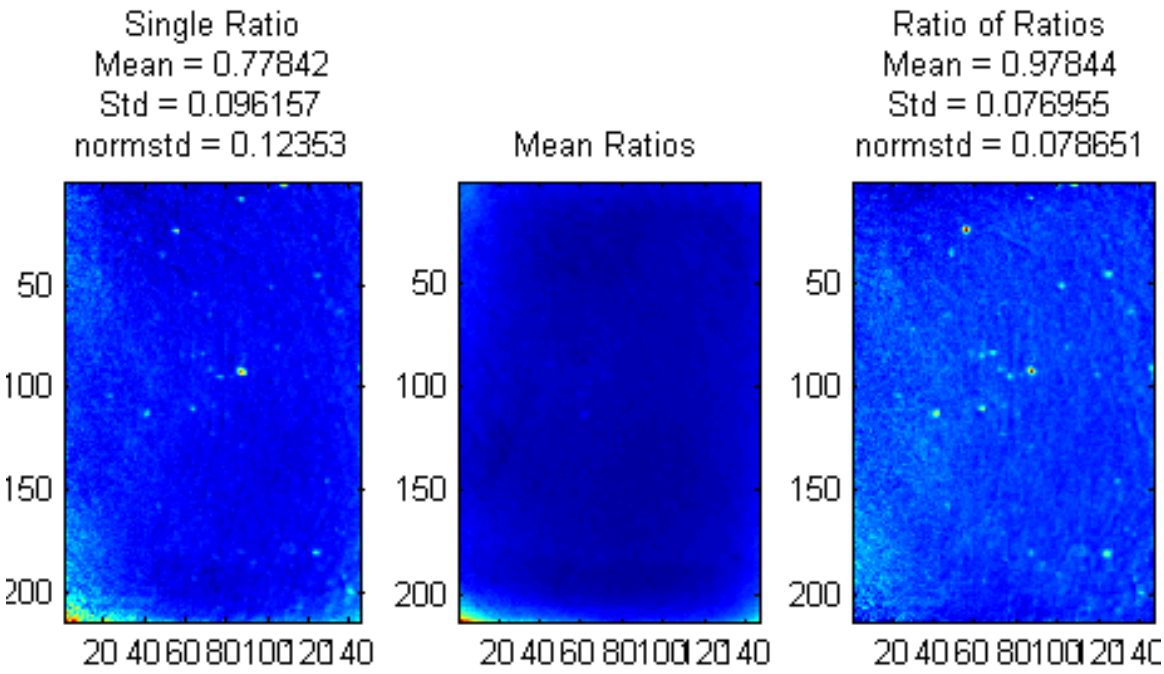

Figure 6.12: Demonstration of correction to the ratio image with the averaged reference

in the ratio due to laser excitation variations across the image.

This variation in ratio due to excitation change is likely due to different responses in the two dyes to changes in excitation intensity. It is clear that the single ratio accounts for much of the spatial laser variation and thus the 2 dyes behave similarly to changes in intensity but not identically. Hence, there is a need for an additional reference or known case to account for the spatial variation.

6.4.2 Dispersed Particle Study

This method proved successful enough with film to warrant further testing on individual particles. Films were made of the brightest particles such that the particles would be visible as independent points of light as opposed to a continuous film of particles. Particles were also dispersed in a water tank and imaged. For this test, a set of particle intensities would be recorded for locations throughout the laser sheet

which would allow for an interpolation of a ratio correction parameter similar to the the film studies before. However, it became clear at this point in the study that the particles were not bright enough on their own for the optical system in use. Only the brightest of the particles registered in the images and it was determined that those were not individual particles (that would display the response times we needed) but rather clumps of particles which showed up brighter than the individual particles.

This indicated to use this optical system, brighter particles needed to be used. The particles in use at the time were developed to be easy to make while still being effective to conduct the tests. They were not as bright as more expensive lab created particles but up until this point in the research had achieved good results in terms of temperature-sensitivity, response time, and accuracy in measuring temperature in the film studies. The brightness of the particles was addressed up until the point were they were visible in our previous tests. The process of making these particles was not adequate in producing particle which were visible through the optical system.

It is important to repeat at this point that the optical system described in Section 6.1 was developed for eventual use in measuring 3-dye particles. For this system, 2 cameras looking through the optical device would be positioned on one side of the subject and 1 camera would be on the other. For a simpler system which requires less light, 2 cameras can be positioned on opposite sides of the subject for measurement of only 2 spectral peaks. This camera setup was subsequently tested in this lab by Pryor[42] which showed good results with pressure sensitive particles.

For temperature-sensitive particles, it was deemed that the particles were still too dim for this setup and research refocused on producing brighter particles. The Bubble Template Method and the Oil/Water/Gas were subsequently investigated as new methods for producing brighter, more uniform temperature particles.

Chapter 7

CONCLUSIONS

A device was developed and used to measure the response times of the various temperature-sensitive dyes and subsequent particle response times. It was found that the temperature response time is dependent on the mass and thickness. By carefully controlling these parameters, it was possible to compare the response times of various dyes. These response times, along with temperature sensitivity and wavelength consideration, were necessary for selecting appropriate dyes for temperature-sensitive particles.

An optical setup was developed to allow for a wide field-of-view images to be taken by two cameras from the same orientation to the subject. The optical system was optimized for flatness of the intensity distribution and for preservation of image quality. The optical system will allow for the utilization of 2, 3, or even 4 camera setups if used in conjunction with another camera setup on the opposite side of the subject. Previous systems used either 2 cameras on opposite sides of the subject or a less advanced optical setup which severely limited field-of-view.

Dual dye particles were tested for spatial uniformity under static conditions and it was found that the single ratio of temperature dye intensity to reference dye intensity was inadequate in producing sufficiently spatially consistent temperature sensors. A ratio-of-ratios was needed to account for the variation in luminescent yield between the two dyes used. Methods were developed to account for this spatial variation which displayed promising results. The synthesis of a wind-off correction image showed that it could account for a large portion of the remaining spatial variation after the ratio of temperature to reference dyes. The remaining variation is likely due to particle

variation and could be solved with more controlled particle production.

Future research should focus on developing brighter particles while not sacrificing the qualities optimized in this research. Brighter particles will allow for better imaging and better temperature data. Future research needs to be conducted to further develop a process for normalizing the laser excitation variation in particle data where a continuous brightness field is not a valid approach. A method for identifying particle brightness and diameter could be used with particle identification software to develop a reference set for this purpose.

BIBLIOGRAPHY

[1] PRN Childs, JR Greenwood, and CA Long. Review of temperature measurement. *Rev. Sci. Instrum.*, 71(8):2959–2978, August 2000.

[2] X Wang, OS Wolfbeis, and RJ Meier. Luminescent probes and sensors for temperature. *Chem. Soc. Rev.*, 42:7834–7869, 2013.

[3] PA Kinzie. *Thermocouple Temperature Measurement*. Wiley, 1973.

[4] AW Van Herwaarden and PM Sarro. Thermal sensors based on the seebeck effect. *Sensors and Actuators*, 10:321–346, 1986.

[5] Majid Nabavi. Unsteady and pulsating pressure and temperature: a review of experimental techniques. *REview of Scientific Instruments*, 81, 2010.

[6] Giovanni Maria Carlomagno and Gennaro Cardone. Infrared thermography for convective heat transfer measurements. *Experiments in Fluids*, 49(6):11871218, Aug 2010.

[7] Simone Zuccher and William S. Saric. Infrared thermography investigations in transitional supersonic boundary layers. *Experiments in Fluids*, 44(1):145157, Sep 2007.

[8] PT Ireland and TV Jones. The response time of a surface thermometer employing encapsulated thermochromic liquid crystals. *J. Phys. E: Sci. Instrum.*, 20:1195–1199, 1987.

[9] PT Ireland and TV Jones. Liquid crystal measurement of heat transfer and surface shear stress. *Meas. Sci. Technol.*, 11:969–986, 2000.

[10] D Dabiri. Digital particle imgae thermometry/velocimetry: a review. *Experimental Fluids*, 46:191–241, 2009.

[11] N Fujisawa and Y Hashizume. An uncertainty analysis of temperature and velocity measured by a liquid crystal visualization technique. *Measurement Science and Technology*, 12(8):1235, 2001.

[12] Innovative scientific solutions, inc. `http://www.psp-tsp.com/`. Accessed: 2014-8-18.

[13] GE Khalil, K Lau, GD Phelan, B Carlson nd M Gouterman, JB Callis, and LR Dalton. Europium beta-diketonate temperature sensors: Effects of ligands, matrix, and concentration. *Review of Scientific Instruments*, 75(1):193–206, January 2004.

[14] BBJ Basu and N Vasantharajan. Temperature dependence of the luminescence lifetime of a europium complex immobilized in different plymer matrices. *Journal of Luminescence*, 128:1701–1708, 2008.

[15] M Lorenz, T Horbach, A Schulz, and HJ Bauer. A novel measuring technique utilizing temperature sensitive paint - measurement procedure, validation, application, and comparison with infrared thermography. *Journal of Turbomachinery*, 135, May 2013.

[16] Y Egami, U Fey, C Klein, J Quest, V Ondrus, and U Beifuss. Development of new two-component temperature-sensitive paint (TSP) for cryogenic testing. *Meas. Sci. Technol.*, 23, 2012.

[17] CY Huang, CA Li, HY Wang, and TM Liou. The application of temperature-sensitive ppaint for surface and fluid temperature measurements in both thermal developing and fully developed regions of a microchannel. *J. Micromech. Microeng.*, 23, 2013.

[18] KJ Disotell, D Peng, TJ Juliano, JW Gregory, JW Crafton, and NM Komerath. Single-shot temperature- and pressure-sensitive paint measurement on an unsteady helicopter blade. *Exp. Fluids*, 55(1671), 2014.

[19] B Dong, B Cao, Y He, Z Liu, Z Li, and Z Feng. Temperature sensing and in vivo imaging by molybdenum sensitized visible upconversion luminescence of rare-earth oxides. *Adv. Mater.*, 24:1987–1993, 2012.

[20] T Tsukamoto, M Esashi, and S Tanaka. High spatial, temporal, and temperature resolution thermal imaging method using $Eu(TTA)_3$ temperature sensitive paint. *J. Micromech. Microeng.*, 23, 2013.

[21] Y Egami, Y Matsuda, H Yamaguchi, and T Niimi. Property changes of temperature-sensitive paint immobilized in acrylic polymer matrices. *Sensors and Actuators: Chemical*, 195:677–681, 2014.

[22] J Brübach, C Pflitsch, A Dreizler, and B Atakan. On surface temperature measurements with thermographic phospors: A review. *Progress in Energy and Combustion Science*, 39:37–60, 2013.

[23] M. Raffel, M. Willert, and J Kompenhans. *Particle Image Velocimetry: A Practical Guide*. Springer-Verlag, Berlin, 1998.

[24] TJ West. Development and testing of temperature-sensitive beads for simultaneous thermometry and velocimetry. Master's thesis, University of Washington, 2012.

[25] D Mishra, PM Lutjen, QS Chen, and V Prasad. Tomographic reconstruction of three-dimensional temperature field using liquid crystal scanning thermography. *Experimental heat transfer*, 13(4):235–258, 2000.

[26] T.S. Pottebaum and M. Gharib. The pinch-off process in a starting buoyant plume. *Experiments in Fluids*, 37(1), Mar 2004.

[27] Satoshi Someya, Satoshi Yoshida, Yanrong Li, and Koji Okamoto. Combined measurement of velocity and temperature distributions in oil based on the luminescent lifetimes of seeded particles. *Meas. Sci. Technol.*, 20, 2009.

[28] S. Someya, D. Ochi, Y. Li, K. Tominaga, K. Ishii, and K. Okamoto. Combined two-dimensional velocity and temperature measurements using a high-speed camera and luminescent particles. *Appl Phys B*, 99:325–332, 2010.

[29] Satoshi Someya, Yanrong Li, Keiko Ishii, and Koji Okamoto. Combined two-dimensional velocity and temperature measurements of natural convection using a high-speed camera and temperature-sensitive particles. *Exp. Fluids*, 50:65–73, 2011.

[30] Daniel Lacroix, Teddy Viraye-Chevalier, Guillaume Seiter, Jonathan Howard, Dana Dabiri, Gamal E. Khalil, Younan Xia, and Cun Zhu. Characterization of multi-dye pressure-sensitive microbeads. *Review of Scientific Instruments*, 84, 2013.

[31] Daniel J Lacroix. Development and characterization of pressure-sensitive microbeads for simultaneous barometry and velocimetry for fluid dynamic applications. Master's thesis, University of Washington, 2014.

[32] Muhammet E Kose. *Multi-luminophore Coatings for Pressure Sensitive Paint Applications*. PhD thesis, University of Florida, 2005.

[33] J.R. Lakowicz. *Principles of Fluorescence Spectroscopy*. Kluwer Academic/-Plenum Publishers, New York, 2nd ed edition, 1999.

[34] Tianshu Liu and John P Sullivan. *Pressure and Temperature Sensitive Paints*. Springer, 2005.

[35] Martin Sommerfeld Yutaka Tsuji Clayton T. Crowe, John D. Schwarzkopf. *Multiphase Flows with Droplets and Particles*. CRC Press, 1997.

[36] Saensuk Wetchagarun and James J. Riley. Dispersion and temperature statistics of inertial particles in isotropic turbulence. *Physics of Fluids*, 22, 2010.

[37] J.G.M. Kuerten B.J. Geurts. A. Bukhvostova, E. Russo. Comparison of dns of compressible and incompressible turbulent droplet-laden heated channel flow with phase transition. *International Journal of Multiphase Flow.*, 63, 2014.

[38] Hirofumi Daiguji, Shingo Takada, Jay J. Molino Cornejo, and Fumio Takemura. Fabrication of hollow poly(lactic acid) microcapsules from microbubble templates. *The Journal of Physical Chemistry B*, 113(45):1500215009, Nov 2009.

[39] JN Demas and GA Crosby. On the multiplicity of the emitting state of ruthenium (ii) complexes. *Journal of Molecular Spectroscopy*, 26(1):72–77, 1968.

[40] Paul C Beaumont, David G Johnson, and Barry J Parsons. Photophysical properties of laser dyes: picosecond laser flash photolysis studies of rhodamine 6g, rhodamine b and rhodamine 101. *Journal of the Chemical Society, Faraday Transactions*, 89(23):4185–4191, 1993.

[41] Sang-Hyun Park and Hyung Jin Sung. Correlation-based image registration for applications using pressure-sensitive paint. *AIAA journal*, 43(3):472–478, 2005.

[42] Lillian Pryor. Development of simultaneous pressure and velocity mmeasurement using multi-luminophore microspheres for wind tunnel application. Master's thesis, University of Washington, 2015.

[43] J Duncan, T Bryce, H Thomsen, D Dabiri, JR Hove, and M Gharib. An extended study of a generalized digital particle image velocimetry (DPIV) processing technique. *Measurement Science and Technology*, 20, 2009.

[44] GE Khalil, C Costin, J Crafton, G Jones, S Grenoble, M Gouterman, JB Callis, and LR Dalton. Dual-luminophor pressure-sensitive paint I. ratio of reference to sensor giving a small temperature dependency. *Sensors and Actuators B*, 97:13–21, 2004.

Appendix A

LUMINESCENT DYE ABSORPTION AND EMISSION SPECTRA

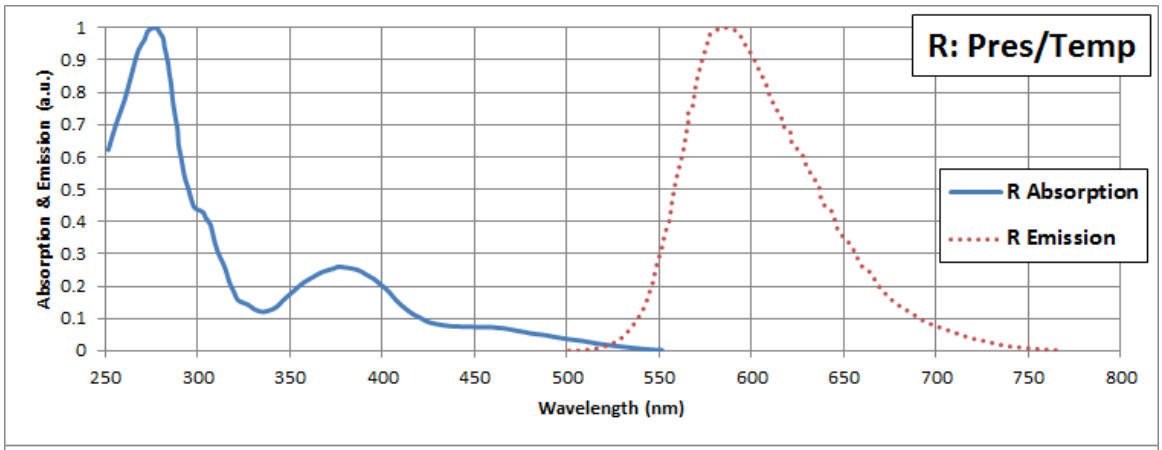

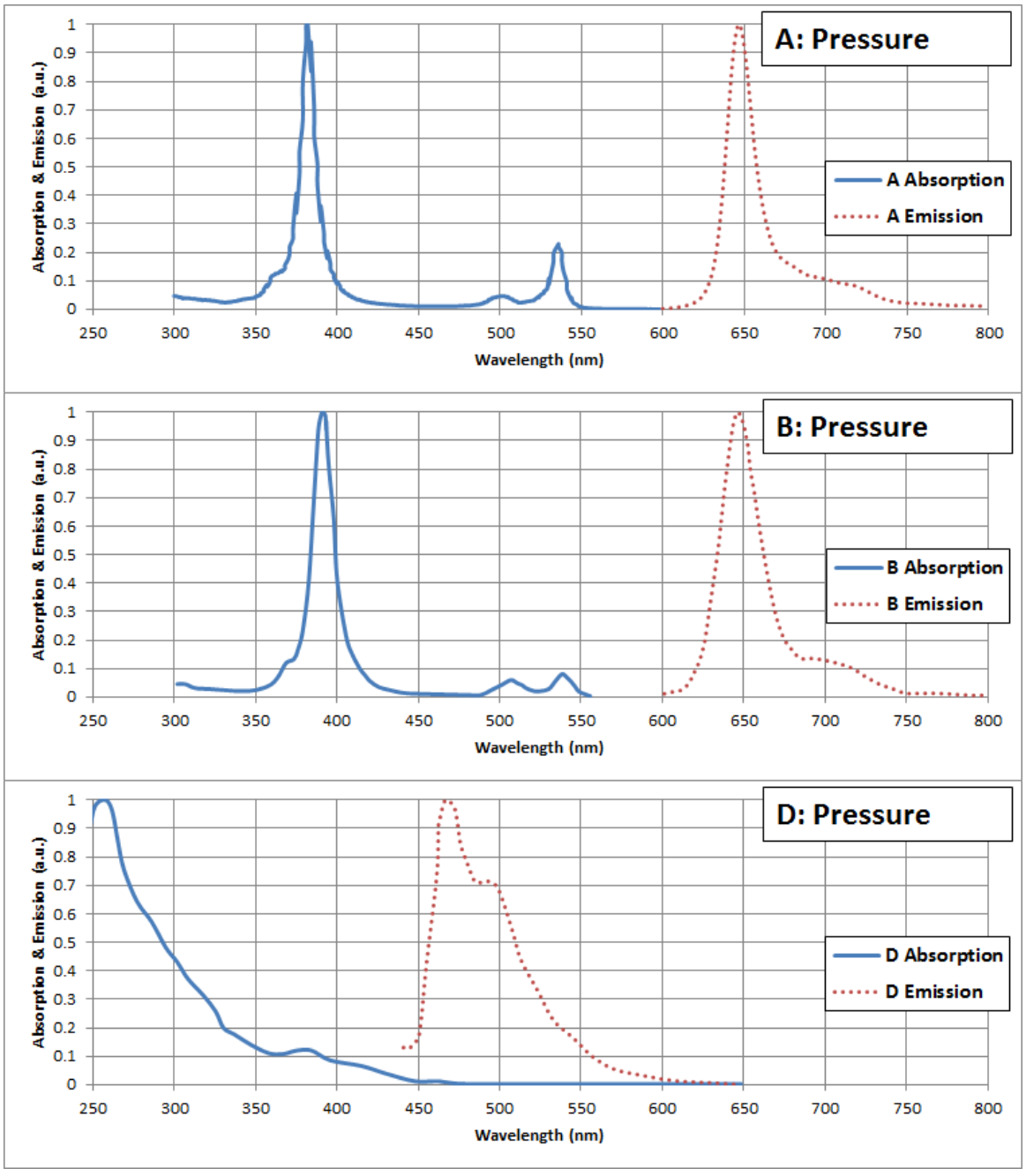
A: Pressure
A Absorption
A Emission
B: Pressure
B Absorption
B Emission
D: Pressure
D Absorption
D Emission
Absorption & Emission (a.u.)
Wavelength (nm)
0
0.1
0.2
0.3
0.4
0.5
0.6
0.7
0.8
0.9
1
250
300
350
400
450
500
550
600
650
700
750
800

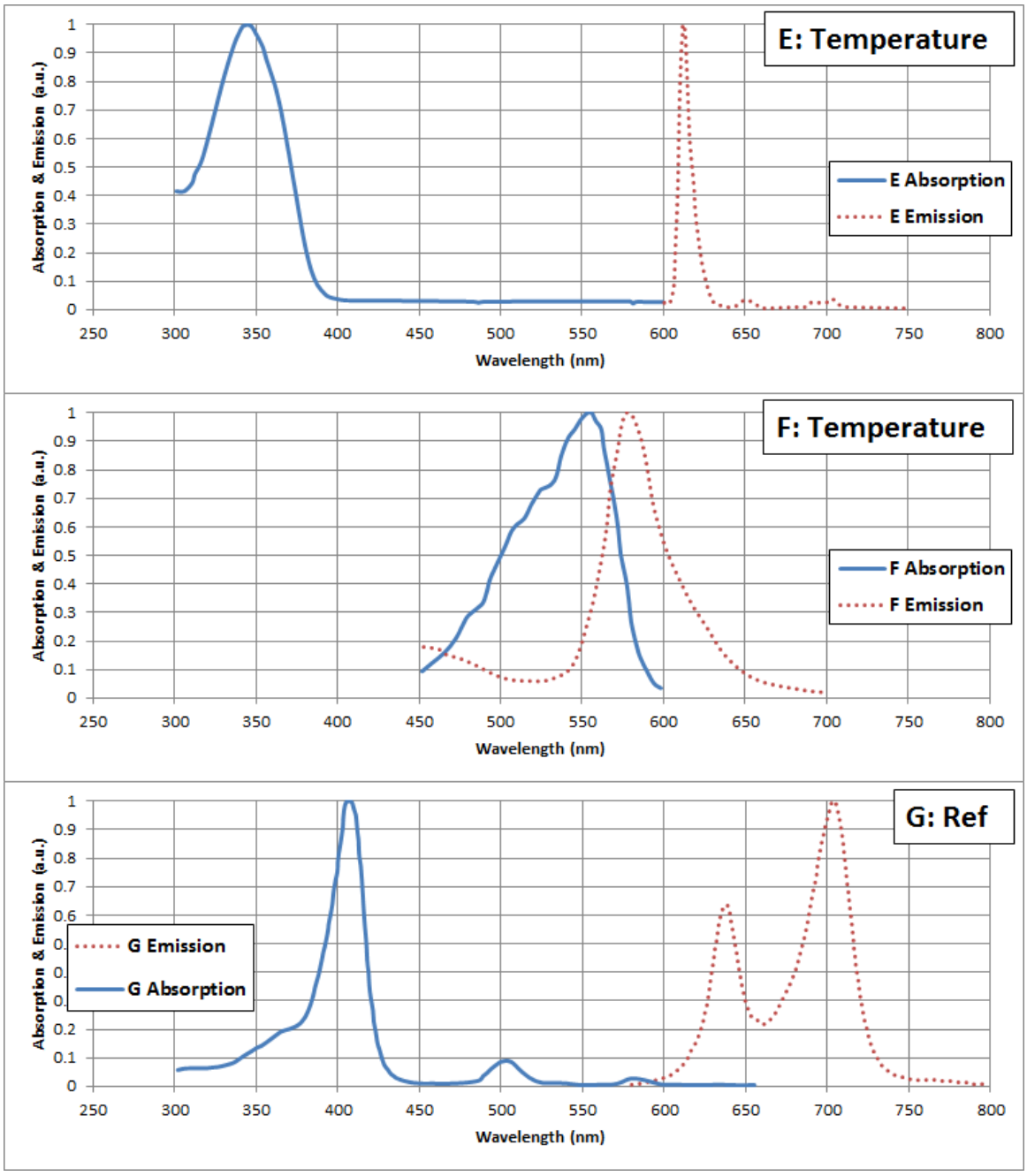
E: Temperature
E Absorption
E Emission
Absorption & Emission (a.u.)
Wavelength (nm)
F: Temperature
F Absorption
F Emission
Absorption & Emission (a.u.)
Wavelength (nm)
G: Ref
G Emission
G Absorption
Absorption & Emission (a.u.)
Wavelength (nm)

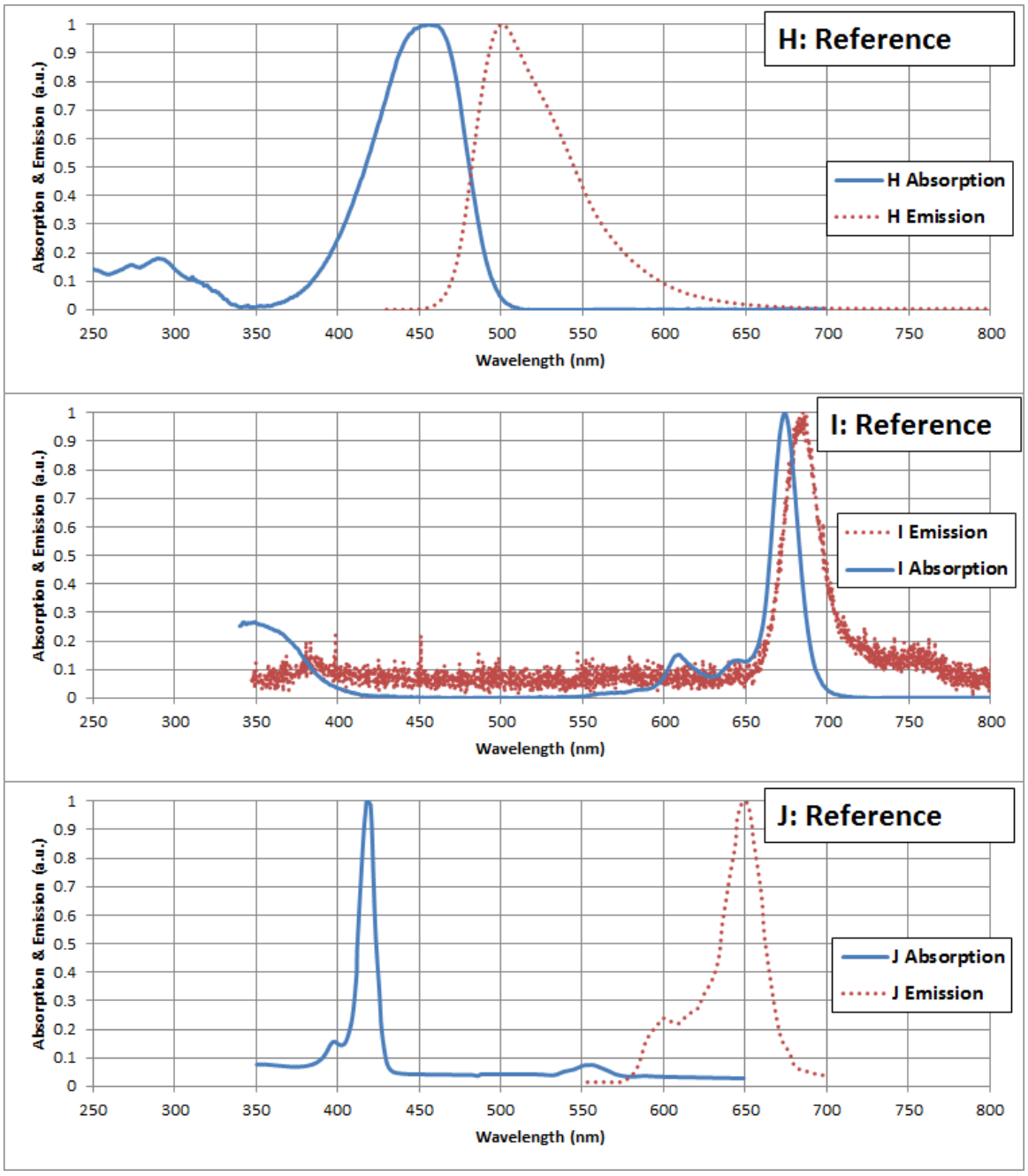
H: Reference
H Absorption
H Emission
Absorption & Emission (a.u.)
Wavelength (nm)
I: Reference
I Emission
I Absorption
Absorption & Emission (a.u.)
Wavelength (nm)
J: Reference
J Absorption
J Emission
Absorption & Emission (a.u.)
Wavelength (nm)

Appendix B

MATLAB CODES FOR IMAGE PROCESSING

```
function [ImagesOut] = FlatFieldCorrect(ImagesIn, Flats, Darks, ...
    Ambients)
%{
    Flat Field Correction Code

    Written by Trey Cottingham, University of Washington
    28 October 2014

    This code takes a series of images in the form uint16 stacked in ...
       a 3-D
    matrix such that for ImagesIn(a,b,c), a and b denote individual ...
       pixels
    in the images and c denotes each image in the stack. Likewise, ...
       Flats,
    Darks, and Ambients are also image stacks of the same form.

    ie. for a series of 200 512x512 images ImagesIn, Flats, Darks, and
    Ambients will all be <512x512x200> in size.

    ImagesOut the flat field corrected series of images in double ...
       format.

    ImagesIn may also be a 4-D matrix where the 4th dimension denotes
    different data points (temperatures, pressures, etc.) In this case,
    ImagesOut will also be a 4-D matrix of the same dimensions.
```

```
%}
    navg=size(ImagesIn,3); % number of frames captured by each camera

    dark_avg = mean(Darks,3);
    ambient_avg = mean(Ambients,3);
    flat_avg = mean(Flats,3);

    G = mean(mean(flat_avg-dark_avg))./(flat_avg-dark_avg);

    %Limit G to account for rare divide by zero cases
    %(Limits G to a finite multiplier)
    G = min(G,20); %20 is chosen as an arbitrary multiplier limit
    G = max(G,0); %Gets rid of G<0

    %This creates matrices of the modification variables so that ...
       they can
    %be applied to the images in arbitary stack sizes and dimensions
    %without the need to loop. This is more efficient.
    G_size = size(ImagesIn);
    G_rep = repmat(G,[1 1 G_size(3:end)]);
    ambient_rep = repmat(ambient_avg,[1 1 G_size(3:end)]);
    ImagesOut=(double(ImagesIn)-ambient_rep).*G_rep;

    %Remove negative intensities from corner vignetting
    %This seems to only happen when the corners in the flatfield go ...
       all the
    %way to dark.
    ImagesOut = max(ImagesOut,0);
```

```
function [x,y,u,v] = ImageReg(img_a, img_b, varargin)
%{
    Image Registration Code

    Written by Trey Cottingham, University of Washington
    28 October 2014
    based on code written by Daniel Lacroix, University of Washington
    uses functions written by Kristian Sveen

    This code takes two images and finds the vector field that describes
    the motion between the two images. This is based on a windowed PIV
    multipass code using cross-correlation of the windows.

    Additional inputs allow  control of final window size (note: initial
    window size will be double this so ensure that these windows ...
       will fit
    in the images), overlap of windows, mask, image mirroring, and ...
       manual
    outlier removal.

    x and y are the locations of the vectors and u and v are the
    displacement vector components for the windows from img_a to img_b.
%}
if(nargin == 2)
    winsize = 32; %Final size of vector windows
    overlap = 0.5; %Overlap for alignment
    mask = []; %Mask to hide parts of image from alignment
    fliplr = false; %if one of the images needs to me mirrored left ...
       to right
    manual = true; %if you want to use manual outlier removal during run
elseif (nargin == 4)
    winsize = varargin{1};
    overlap = varargin{2};
```

```
31      mask = [];
32      fliplr = flase;
33      manual = true;
34  elseif (nargin == 6)
35      winsize = varargin{1};
36      overlap = varargin{2};
37      mask = varargin{3};
38      fliplr = varargin{4};
39      manual = true;
40  elseif (nargin == 7)
41      winsize = varargin{1};
42      overlap = varargin{2};
43      mask = varargin{3};
44      fliplr = varargin{4};
45      manual = varargin{5};
46  end
47
48
49      if size(img_a)~=size(img_b) % Different size images
50          img_a=imresize(img_a,size(img_b));%resizing for PIV
51          img_b=img_b.*(max(img_a)/max(img_b)); %scale intensities
52      end
53
54      Dt=1;  %piv code parameter
55      [x,y,u,v,SnR,Pkh]=multipass(img_a,img_b,winsize*2,Dt,overlap,mask);
56      u(abs(u)>50|abs(v)>50)=NaN; v(abs(u)>50|abs(v)>50)=NaN; % hard ...
            remove outliers
57      figure(4), quiver(x,y,u,v), axis tight
58
59      % option to use manual outlier removal before actual ...
            outlier_removal code
60
61      if manual;
```

```
62          h=msgbox('Press "RETURN" when done','Manual Outlier ...
                Removal'); pause(1)
63          if ishandle(h); close(h); end; % if message still active ...
                close it
64          loop=1;
65          while loop==1
66              [xx,yy]=ginput; % if yes then get clicks for bad piv arrows
67              for i=1:length(xx) % for each click
68                  remov=find(abs(x-xx(i))==min(min(abs(x-xx(i)))) & ...
69                      abs(y-yy(i))==min(min(abs(y-yy(i))))); % match ...
                            click to u and v
70                  u(remov)=NaN; v(remov)=NaN;
71              end
72              figure(4), quiver(x,y,u,v), axis tight
73              chc = questdlg('Continue Manual Outlier ...
                    Removal?','Outlier Removal');
74              if strcmp(chc,'No'); loop=0; elseif ...
                    strcmp(chc,'Cancel'); break; end
75          end
76      end
77      [u,v,I1] = outlier_removal(u,v,0.5); % remove outliers to smooth ...
            piv data
78
79      figure(4), quiver(x,y,u,v), axis tight
80      set(gca,'YDir','reverse');
81  end
```

```
function [Img_I] = interpolation(Img, x, y, u, v)
%{
Interpolation of Image Data

Written by Trey Cottingham, University of Washington
28 October 2014

This code takes an image and vector field displacement to find ...
    proper pixel
values for the output Img_I based off of discrete pixel values Img ...
    and the
displacements in [U,V] at [x,y].

The discrete vector field given in (x,y,u,v) is interpolatd to every ...
    pixel
in Img and then new intensity values are calculated with a cubic
interpolation.

Img can be a single image or a image stack with
    size <xlength x ylength x f_max>
%}

%find width of image
xlength=size(Img,1);
ylength=size(Img,2);
f_max = size(Img,3);

%reshape vector data to columns
u_ = u(:);
v_ = v(:);
x_ = x(:);
y_ = y(:);

```

```
31 [XXgrid YYgrid] = meshgrid(1:xlength,1:ylength);
32
33 %Interpolate vector field to every pixel in Img
34 u_I = ...
       reshape(griddata(x_,y_,u_,XXgrid(:),YYgrid(:),'cubic'),ylength,xlength);
35 display('Horizontal Vectors Interpolated')
36 v_I = ...
       reshape(griddata(x_,y_,v_,XXgrid(:),YYgrid(:),'cubic'),ylength,xlength);
37 display('Vertical Vectors Interpolated')
38
39 %New pixel coordinates to be interpolated for Img_I
40 XX_I = XXgrid + u_I;
41 YY_I = YYgrid + v_I;
42
43 Img_I = zeros(ylength,xlength,f_max);
44 for i = 1:f_max
45 %cubic interpolation
46     Img_I(:,:,i) = ...
           interp2(XXgrid,YYgrid,double(Img(:,:,i)),XX_I,YY_I,'cubic');
47 end
48 end
```

Appendix C

CIRCUIT DOCUMENTATION

Written by Roy Olund

included with permission from author

Circuit Description

The circuit consists of five basic components: the energy storage capacitors, the heating element, a fast switch, a voltage sensing and scaling amplifier and a current sensing and scaling amplifier. The circuit is shown in the figure below.

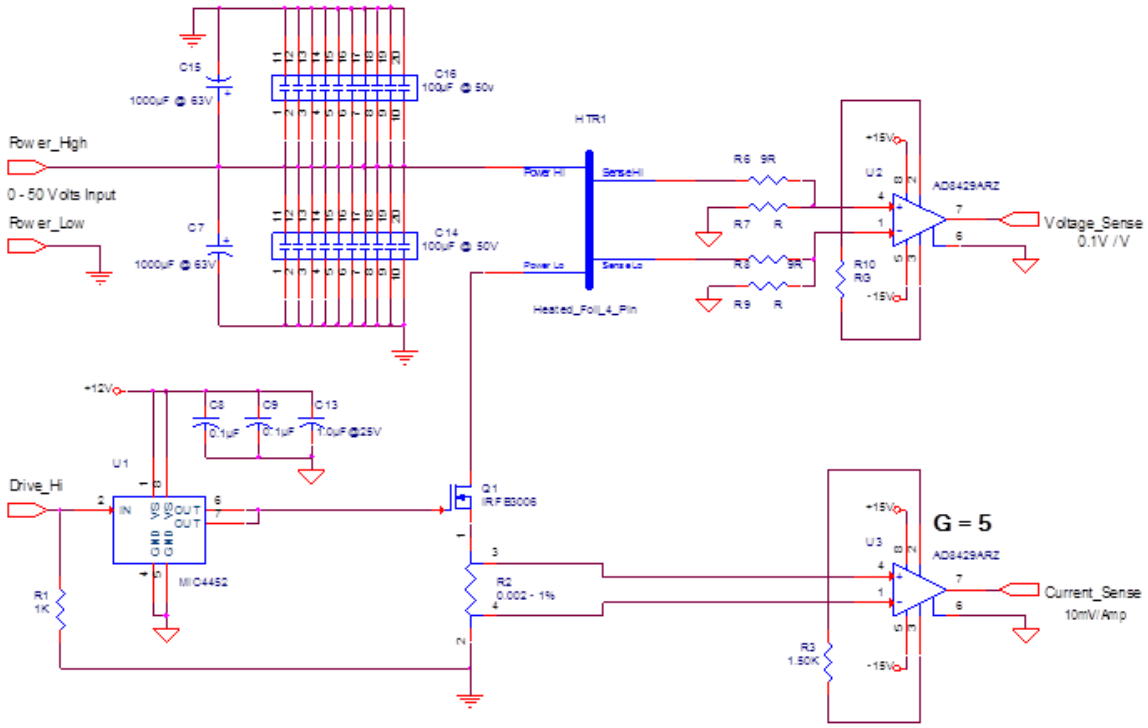

The energy storage consists of C7, C14, C15 and C16. C14 and C16 are arrays of ceramic capacitors and provide the charge needed for the fast switching transients

of several hundred amperes. C7 and C15 help isolate the power supply from the load. The Power Supply has a range of 0 to 50 Volts maximum. The heating element consists of a thin (25m) strip of titanium clamped by copper elements. This is wired into the circuit as a four terminal Kelvin sensing/load resistor. The switch consists of a very low on resistance (2.1 milli-ohm) FET (Q1). The gate is driven by the IC (U1) which is capable of providing a peak gate current of 12A. The FET is capable of passing 1000 amps peak current. The heater current is sensed by the 2.0 milli-ohm four lead resistor R2. The sensed voltage is amplified by U3 to provide an output signal of 10 mV per amp. The heater voltage is sensed by the matched dividers R6 R7 and R8 R9 and amplified by U3 to produce an output signal of 0.1 volts per volt of heater voltage.

Temperature Determination

The temperature can be determined by computing the resistance as a function of time. The voltage across and the current through the load can be acquired with a sampling digital oscilloscope or with a fast data acquisition system. If an oscilloscope is used a pulse is acquired and stored and the voltage and current are measured with the cursor function of the oscilloscope at a few points spanning the pulse. The resistance can be computed from the ratio. The temperature change is then computed from the temperature coefficient of resistance of the titanium strip. The initial temperature of the strip is assumed to be room temperature and the change is added to this temperature. If a data acquisition system is used, the temperature can be computed and displayed as a time domain plot as the data is acquired.

Heating Rate

The Heating Rate is computed from the input power and the physical parameters of the heated strip.

1. The input power is computed from: $Heat = I^2 * R * time$.
2. The temperature rise is computed from: $\Delta T = \frac{Heat}{(mass * C_p)}$.
3. Substituting: $R = \frac{r * length}{Area}$.
4. And: $mass = \rho * length * Area$.
5. And: Heating rate: $\frac{dT}{dt} = \frac{\Delta T}{time}$.
6. Gives a Rate Equation: $\frac{dT}{dt} = \frac{I^2 * r}{Area^2 ** C_p}$.
7. Where all parameters are in MKS units.
8. A heating merit quantity can be defined as: $K_{Heating} = \frac{r}{\rho * C_p}$.
9. This gives: $\frac{dT}{dt} = K_{Heating} * [Currentdensity]^2$
10. A table of Material Properties is given below:

Metal	Resistivity	Temp Coeff of R	Density	Specific Heat	$K_{heating}$
	$\mu\Omega\,\mathrm{cm}$	$^{\circ}\mathrm{C}^{-1}$	$\mathrm{kg/m^3}$	$\mathrm{J\,K^{-1}\,kg}$	
Aluminum	2.67	0.0045	2700	900	1.1
Beryllium	3.3	0.009	1848	1825	0.98
Chromium	13.2	0.00214	7100	518	3.59
Cobalt	6.34	0.0066	8900	456	1.56
Copper	1.69	0.0043	8960	385	0.49
Gold	2.2	0.004	19300	129	0.88
Indium	8.8	0.0052	7300	234	5.15
Iridium	5.1	0.0045	22400	133	1.71
Iron	10.1	0.0065	7870	444	2.89
Molybdenum	5.7	0.00435	10220	251	2.22
Nickel	6.9	0.0068	8900	444	1.75
Palladium	10.8	0.0042	12000	244	3.69
Platinum	10.58	0.00392	21450	133	3.71
Silver	1.63	0.0041	10500	237	0.66
Tantalum	13.5	0.0035	16600	140	5.81
Tin	12.6	0.0046	7280	213	8.13
Titanium	54	0.0038	4500	523	22.94
Tungsten	5.4	0.0048	19300	133	2.1
Zinc	5.96	0.0042	7140	388	2.15
Zirconium	44	0.0044	6490	281	24.13
Stainless Shim	21	0.0013	7800	500	5.38

This data was obtained from the Goodfellow Metals Catalog (www.goodfellowusa.com). Titanium and Zirconium are clearly the optimum metals for heating speed with titanium being the one available in the largest variety of forms.